Monthly Notices
of the
ROYAL ASTRONOMICAL SOCIETY

MNRAS **445,** 3133–3151 (2014) doi:10.1093/mnras/stu1948

Constraining the Galaxy's dark halo with RAVE stars

T. Piffl,[1⋆] J. Binney,[1] P. J. McMillan,[1] M. Steinmetz,[2] A. Helmi,[3] R. F. G. Wyse,[4] O. Bienaymé,[5] J. Bland-Hawthorn,[6] K. Freeman,[7] B. Gibson,[8,9] G. Gilmore,[10] E. K. Grebel,[11] G. Kordopatis,[10] J. F. Navarro,[12†] Q. Parker,[13,14,15] W. A. Reid,[13,14] G. Seabroke,[16] A. Siebert,[5] F. Watson[15] and T. Zwitter[17,18]

[1]*Rudolf Peierls Centre for Theoretical Physics, Keble Road, Oxford OX1 3NP, UK*
[2]*Leibniz-Institut für Astrophysik Potsdam (AIP), An der Sternwarte 16, D-14482 Potsdam, Germany*
[3]*Kapteyn Astronomical Institute, University of Groningen, PO Box 800, NL-9700 AV Groningen, the Netherlands*
[4]*Department of Physics & Astronomy, Johns Hopkins University, Baltimore, MD 21218, USA*
[5]*Observatoire astronomique de Strasbourg, UMR 7550 CNRS/Université de Strasbourg, F-67000 Strasbourg, France*
[6]*Sydney Institute for Astronomy, University of Sydney, NSW 2006, Australia*
[7]*Research School of Astronomy and Astrophysics, Australian National University, Cotter Rd, Weston, ACT 2611, Australia*
[8]*Institute for Computational Astrophysics, Department of Astronomy & Physics, Saint Mary's University, Halifax, NS BH3 3C3, Canada*
[9]*Jeremiah Horrocks Institute, University of Central Lancashire, Preston PR1 2HE, UK*
[10]*Institute for Astronomy, University of Cambridge, Madingley Road, Cambridge CB3 0HA, UK*
[11]*Astronomisches Rechen-Institut, Zentrum für Astronomie der Universität Heidelberg, Mönchhofstr. 12–14, D-69120 Heidelberg, Germany*
[12]*Department of Physics and Astronomy, University of Victoria, Victoria, BC V8P 5C2, Canada*
[13]*Department of Physics, Macquarie University, Sydney, NSW 2109, Australia*
[14]*Research Centre for Astronomy, Astrophysics and Astrophotonics, Macquarie University, Sydney, NSW 2109, Australia*
[15]*Australian Astronomical Observatory, PO Box 915, North Ryde, NSW 1670, Australia*
[16]*Mullard Space Science Laboratory, University College London, Holmbury St Mary, Dorking, RH5 6NT, UK*
[17]*Faculty of Mathematics and Physics, University of Ljubljana, Jadranska 19, 1000 Ljubljana, Slovenia*
[18]*Center of excellence space-si, Askerceva 12, 1000 Ljubljana, Slovenia*

Accepted 2014 September 16. Received 2014 September 11; in original form 2014 June 14

ABSTRACT

We use the kinematics of ∼200 000 giant stars that lie within ∼1.5 kpc of the plane to measure the vertical profile of mass density near the Sun. We find that the dark mass contained within the isodensity surface of the dark halo that passes through the Sun ($(6 \pm 0.9) \times 10^{10}\,\mathrm{M}_\odot$), and the surface density within 0.9 kpc of the plane ($(69 \pm 10)\,\mathrm{M}_\odot\ \mathrm{pc}^{-2}$) are almost independent of the (oblate) halo's axis ratio q. If the halo is spherical, 46 per cent of the radial force on the Sun is provided by baryons, and only 4.3 per cent of the Galaxy's mass is baryonic. If the halo is flattened, the baryons contribute even less strongly to the local radial force and to the Galaxy's mass. The dark matter density at the location of the Sun is $0.0126\,q^{-0.89}\,\mathrm{M}_\odot\ \mathrm{pc}^{-3} = 0.48\,q^{-0.89}\,\mathrm{GeV\,cm}^{-3}$. When combined with other literature results we find hints for a mildly oblate dark halo with $q \simeq 0.8$. Our value for the dark mass within the solar radius is larger than that predicted by cosmological dark-matter-only simulations but in good agreement with simulations once the effects of baryonic infall are taken into account. Our mass models consist of three double-exponential discs, an oblate bulge and a Navarro–Frenk–White dark matter halo, and we model the dynamics of the RAVE (RAdial Velocity Experiment) stars in the corresponding gravitational fields by finding distribution functions $f(\boldsymbol{J})$ that depend on three action integrals. Statistical errors are completely swamped by systematic uncertainties, the most important of which are the distance to the stars in the photometric and spectroscopic samples and the solar distance to the Galactic Centre. Systematics other than the flattening of the dark halo yield overall uncertainties ∼15 per cent.

Key words: Galaxy: disc – Galaxy: fundamental parameters – Galaxy: halo – Galaxy: kinematics and dynamics – solar neighbourhood – Galaxy: structure.

⋆ E-mail: tilmann.piffl@physics.ox.ac.uk
† Senior CIfAR Fellow.

© 2014 The Authors
Published by Oxford University Press on behalf of the Royal Astronomical Society
Downloaded from https://academic.oup.com/mnras/article-abstract/445/3/3133/1052064
by University of Hull user
on 29 June 2018

1 INTRODUCTION

There is abundant evidence that haloes of still undetected dark matter dominate the mass budgets of galaxies. Galaxies with luminosities similar to that of the Milky Way have the largest baryon fractions, yet even in these systems we think there is at least an order of magnitude more dark matter than stars and gas. This belief is founded on numerous lines of evidence, but two important and essentially independent ones are the dynamics of the Local Group (Kahn & Woltjer 1959; Li & White 2008) and fits of ΛCDM cosmologies to the cosmic background radiation combined with numerical simulations of galaxy formation (e.g. Bower et al. 2010).

Since attempts to detect dark matter through its weak interactions in underground experiments have yet to bear fruit (Mirabolfathi 2013), dark matter is so far only detectable through its gravitational field. Studies of weak lensing (Velander et al. 2014) and thermal X-ray emission (Das et al. 2011) have been used to map dark matter on large scales, while the kinematics of stars and gas provide the most powerful probe on small scales. For intermediate regions, strong lensing can provide some insights (e.g. Kneib & Natarajan 2011).

Studies of star and gas kinematics in our own Milky Way have to date constrained the dark matter distribution less strongly than have similar studies in external galaxies, such as NGC 3198 (van Albada et al. 1985). The cause of this surprising fact is essentially that dark matter is most important at large radii, where it becomes difficult to determine distances to objects with measured velocities. Moreover, the Sun's velocity and location with respect to the Galactic Centre (GC) has an uncertainty of several per cent, and this uncertainty propagates to the Galactocentric velocities of all tracers, which are inevitably measured in the heliocentric frame.

It is thought that of order half the inward force on the Sun derives from dark matter and half from stars and gas, predominantly in the disc (Sackett 1997). A significant step towards testing this conviction would be to show that the structure of the Galaxy's gravitational field perpendicular to the plane is consistent with roughly half the mass interior to the Sun being contained in the disc and the other half contained in a roughly spherical halo (e.g. Sackett 1997). One of the original goals of the RAdial Velocity Experiment (RAVE; Steinmetz et al. 2006) was to test this hypothesis by gathering spectra of large numbers of stars within the 'extended solar neighbourhood', the region within ∼2 kpc of the Sun. In this paper, we describe our attempt in this direction. The independent parallel work by Bienaymé, Famaey & Siebert (2014) has similar goals, but a very different methodology. Recently, also the *SEGUE* survey (Yanny et al. 2009) was used by Zhang et al. (2013) to estimate the local dark matter density.

The fourth data release from RAVE gives line-of-sight velocities and stellar parameters for ∼400 000 stars in the extended solar neighbourhood (Kordopatis et al. 2013). Using these stellar parameters, Binney et al. (2014a) estimated distances to the stars, which are roughly half giants and half dwarfs. Combining the RAVE data with proper motions from the UCAC4 (Zacharias et al. 2013), Binney et al. (2014b) derived the velocity distributions of stars in eight spatial bins, four inside the solar radius R_0 and four outside it, and at various distances from the plane. They showed that these velocity distributions were in remarkably good agreement with those predicted by a dynamical model of the Galaxy that Binney (2012b, hereafter B12b) had fitted to the velocity distribution at the Sun determined by the Geneva–Copenhagen survey (hereafter GCS; Nordström et al. 2004; Holmberg, Nordström & Andersen 2007) and the estimate of density versus distance from the plane derived by Gilmore & Reid (1983).

Although the agreement between data and model was near perfect near the plane, at distances $|z| \gtrsim 0.5$ kpc the model failed to reproduce the data in two respects: (i) the distribution of the components V_1 of velocity parallel to the longest principal axis of the velocity ellipsoid (which points near to the GC) was predicted to be too narrow; (ii) the predicted distribution of azimuthal components V_ϕ tended to be slightly displaced to small V_ϕ with respect to the observed distribution. Neither defect is an inherent feature of an axisymmetric equilibrium model.

In this paper, we have two goals: (i) to seek a modified form of the distribution function (DF) of the B12b model that is consistent with the RAVE data, and (ii) to use models obtained in this way to constrain the local gravitational field and thus the distribution of dark matter.

2 DATA

In this section, we introduce the data we have used and explain how we exploited them to constrain our Galaxy model. In order to make model predictions for these measurements, we assume a distance of the Sun to the GC, R_0, to be 8.3 kpc (e.g. Gillessen et al. 2009; McMillan 2011; Schönrich 2012), the position of the Sun above the Galactic plane, z_0, to be 14 pc (Binney, Gerhard & Spergel 1997) and the solar motion with respect to the local standard of rest (LSR), $\boldsymbol{v}_\odot$, to be (11.1, 12.24, 7.25) km s^{-1} (Schönrich, Binney & Dehnen 2010).

2.1 Gas terminal velocities

The distribution of H I and CO emission in the longitude-velocity plane yield a characteristic maximum ('terminal') velocity for each line of sight (e.g. Binney & Merrifield 1998, section 9.1.1). The terminal velocities are related to the circular speed $v_c(R)$ by

$$\begin{aligned} v_{\rm term}(l) &= \mathrm{sign}(\sin l) v_c(R) - v_c(R_0)\sin l \\ &= \mathrm{sign}(\sin l) v_c(R_0|\sin l|) - v_c(R_0)\sin l. \end{aligned} \quad (1)$$

We use the terminal velocities $v_{\rm term}(l)$ from Malhotra (1995). Following Dehnen & Binney (1998) and McMillan (2011), we neglect data at $\sin l < 0.5$ in order not to be influenced by the Galactic bar, and we assume that the ISM has a Gaussian velocity distribution of dispersion 7 km s^{-1}.

2.2 Maser observations

Reid et al. (2014) presented a compilation of 103 maser observations that provide precise 6D phase space information. Since masers are associated with young stars their motions are very close to circular around the GC. We again assume an intrinsic velocity dispersion of 7 km s^{-1} and no lag against the circular speed (McMillan & Binney 2010). For the likelihood computation we neglected 15 sources that were flagged as outliers by Reid et al. (2014) and also all sources at $R < 4$ kpc. The latter is again to prevent a bias by the Galactic bar. To assess the likelihood of a maser observation, we predict the observed velocities (line-of-sight velocity, proper motions) as functions of heliocentric distance and then integrate the resulting probability density along the line of sight.

Downloaded from https://academic.oup.com/mnras/article-abstract/445/3/3133/1052064
by University of Hull user
on 29 June 2018

2.3 Proper motion of SgrA*

Reid & Brunthaler (2004) measured the proper motion of the radio source SgrA* in the GC to be

$$\mu_{\mathrm{SgrA}^\star} = -6.379 \pm 0.024\,\mathrm{mas\,yr^{-1}}.$$

This source is thought to be associated with the supermassive black hole that sits in the gravitational centre of the Milky Way with a velocity below 1 km s^{-1}. Hence, this measurement reflects the solar motion with respect to the GC.

2.4 Mass within 50 kpc

By modelling the kinematics of the Galaxy's satellites, Wilkinson & Evans (1999) estimated the mass of the Galaxy within 50 kpc to be

$$M(r < 50\,\mathrm{kpc}) = 5.4^{+0.2}_{-3.2} \times 10^{11}\,\mathrm{M}_\odot.$$

Following McMillan (2011), we use this measurement as an upper limit on the mass of our models. This limit effectively sets the scale radius $r_{0,\,\mathrm{dm}}$ of the halo because all plausible models have $M(r < 50\,\mathrm{kpc})$ very close to the Wilkinson & Evans' upper limit.

2.5 Concentration of the dark halo

The dark halo has two free parameters: the normalizing density $\rho_{0,\,\mathrm{dm}}$ and the scale radius $r_{0,\,\mathrm{dm}}$. We constrain the scale radius using the most likely value for the concentration parameter c as found in cosmological dark-matter-only simulations. The normalizing density of the dark halo is

$$\rho_{0,\mathrm{dm}} = \frac{3H^2}{8\pi G}\delta_c, \tag{2}$$

where δ_c is related to the halo's concentration parameter c by

$$\delta_c = \frac{\Delta_{\mathrm{vir}}}{3}\frac{c^3}{\ln(1+c) - c/(1+c)}, \tag{3}$$

with the parameter Δ_{vir} being the virial overdensity. We take the Hubble constant to be $H = 73\,\mathrm{km\,s^{-1}\,s^{-1}\,Mpc^{-1}}$, and from Boylan-Kolchin et al. (2010) adopt

$$\Delta_{\mathrm{vir}} = 94$$

$$\ln c = 2.256 \pm 0.272. \tag{4}$$

With these choices, the local dark matter density $\rho_{\mathrm{dm}}(R_0, z_0)$ becomes a function of only the dark-halo's scale radius $r_{0,\,\mathrm{dm}}$, so the latter can be determined once we have chosen $\rho_{\mathrm{dm}}(R_0, z_0)$.

2.5.1 *Baryon fraction*

By matching the number density of SDSS galaxies with different stellar masses to that of dark matter haloes in the Millennium simulations, Guo et al. (2010) obtained a relation between stellar mass $M_\star$ and M_{200}, the mass interior to a Galactocentric sphere within which the mean density 200 times the critical density for closure of the Universe. Their relation is

$$M_\star = M_{200} \times A\left[\left(\frac{M_{200}}{M_0}\right)^{-\alpha} + \left(\frac{M_{200}}{M_0}\right)^{\beta}\right]^{-\gamma}, \tag{5}$$

where $M_0 = 10^{11.4}\,\mathrm{M}_\odot$, $A = 0.129$, $\alpha = 0.926$, $\beta = 0.261$ and $\gamma = 2.440$. We have imposed this constraint with uncertainty 0.2 in $\log_{10} M_\star$.

2.6 The RAVE survey

The RAVE survey has taken spectra at resolution $R \simeq 7500$ of ∼500 000 stars that have 2MASS photometry. Stars were selected for observation based on their I-band apparent magnitudes; $I \approx 9$–13. Stellar parameters were extracted from the spectra by a pipeline described in Kordopatis et al. (2013), and from those parameters and the 2MASS photometry Binney et al. (2014a) determined probability density functions (pdfs) for the distances of most stars. Roughly half the stars are giants, and these stars form our main sample. Within the survey's observing cone, the giants sample densely the region within ∼2 kpc of the Sun, so they are ideally suited for determination of the vertical structure of the Galaxy's disc. Binney et al. (2014b) examine the kinematics of these stars in some detail.

We clean the data using the following criteria:

(i) Signal-to-noise ratio (S/N) >10.
(ii) For stars with multiple observations, we chose the observation with the highest S/N.
(iii) The stars have a parallax estimate in Binney et al. (2014a).
(iv) Proper motion uncertainty <8 mas yr^{-1}.
(v) $|U|$ and $|W|$ velocity components <350 km s^{-1}.
(vi) The stars lie in the cylindrical shell around the Galactic centre $|R - R_0| < 1$ kpc.

The restrictions in the U and W velocities were introduced to weed out unreliable proper motion and distance estimates. The last criterion selects for relatively nearby stars in RAVE for which we have more trust in the distance estimations. Note that throughout this study we do not look at the azimuthal positions of the stars w.r.t. the GC and hence implicitly assume axisymmetry (as we will do in our Galaxy model). This is, of course, an approximation, as there is known sub-structure in the local stellar population (Dehnen 1998; Antoja et al. 2012; Siebert et al. 2012; Williams et al. 2013).

We then define a sample of giant stars through

$$\log g < 3.5\ \mathrm{dex}.$$

This leaves us with a sample of 181 621 stars. For later use, we also define a sample of hot dwarf stars using the following cuts:

$$\log g > 3.5\ \mathrm{dex},$$
$$T_{\mathrm{eff}} > 6000\,\mathrm{K}.$$

Here, we obtain a sample of 55 398 stars.

2.7 The vertical stellar density profile

Any dynamical mass measurement requires knowledge of the spatial distribution of a tracer population in addition to knowledge of that population's kinematics. Hence, we need an estimate of the spatial distribution of the population from which RAVE stars are drawn. The seminal study of Gilmore & Reid (1983) provided an estimate of the vertical density profile of dwarf stars that remains valuable even though it is based on observations of only ∼2700 objects.[1] More recent data sources include the 2MASS catalogue and the Sloan Digital Sky Survey (SDSS; York et al. 2000). In a subsequent paper, we will constrain the Galaxy's mass distribution by combining RAVE data with star counts from both 2MASS and SDSS: use of both surveys is desirable because the magnitude limit of 2MASS is too bright to give sensitivity to the thick disc, and the

[1] Their estimate for stars with $M_V \in [3, 4]$.

Downloaded from https://academic.oup.com/mnras/article-abstract/445/3/3133/1052064
by University of Hull user
on 29 June 2018

magnitude limit of SDSS is too faint to give sensitivity to the thin disc.

However, here we adopt a less sophisticated approach based on the vertical density profile that Jurić et al. (2008, hereafter J08) deduced from the SDSS survey through a main-sequence colour–magnitude relation. We use the data points shown in the middle panel of their fig. 1 5, which shows results from M dwarf stars in the colour range $0.70 < r - i < 0.80$. Similar to RAVE, this sample should carry only a weak metallicity bias and none in age. J08 fitted their data with the density profile

$$\nu(R = R_0, z) \propto \exp(-|z|/z_{\rm thn}) + f_{\rm thk} \exp(-|z|/z_{\rm thk}) \quad (6)$$

and used artificial star tests to estimate the impact of Malmquist bias and stellar multiplicity on the fitted density profile. They concluded that the fitted scaleheights of both the thin and the thick disc have to be increased $5 + 15 = 20$ per cent to compensate for the two effects, while the parameter $f_{\rm thk}$ that sets the relative importance of the discs, should be decreased by 10 per cent. This results in $z_{\rm thn} = 0.3$ kpc, $z_{\rm thk} = 0.9$ kpc and $f_{\rm thk} = 0.12$.

Here, the Malmquist bias refers to the fact that in the presence of random errors in the apparent and/or the absolute magnitudes of stars – i.e. effectively in their distance moduli μ – their distance estimates will be on average too small. The stars in J08 have magnitude-dependent photometric uncertainties of 0.02–0.12 dex and there is an uncertainty in the estimates of the absolute magnitude coming from the finite width of the main sequence that is not covered by J08's colour–magnitude relation.

Before we compare the data to our predictions, we have to introduce these biases into the model. The Malmquist bias is modelled by folding the vertical stellar number count profile $N(z) \propto 2\pi z^2 \nu(R_0, z)$ with a Gaussian of width 0.32 dex in distance modulus μ. This width is a combination (in quadrature) of the maximal measurement uncertainty of 0.12 dex and a value 0.3 dex for the finite width of the main sequence. For stellar multiplicity, the modelling is more uncertain. We use the simplifying assumptions that (1) we have only binaries and (2) that the companions have about the same brightness as the primaries as such systems occur preferentially (Delfosse et al. 2004) and also produce most of the effect. This results in an underestimate of their true distance by a factor of $1/\sqrt{2}$. The resulting new profile $N'(z)$ is then computed from the original profile $N(z)$ as follows:

$$N'(z) = (1 - f_{\rm binary})N(z) + f_{\rm binary} N(\sqrt{2}z), \quad (7)$$

where $f_{\rm binary}$ is the binary fraction. The biased number count profile is then converted back into a density profile $\propto N'(z)/(2\pi z^2)$. Dieterich et al. (2012) report a fraction of about 10 per cent of M dwarfs having M dwarfs companions and we adopt this number. Fig. 1 illustrates the effect of the two biases. Note that J08 assumed higher binary fraction of 35 per cent to correct their fit results. This led to more significant corrections than those applied here. The differences are well within the range of systematic uncertainties reported below.

3 METHODOLOGY

For a number of candidate mass distributions and associated gravitational potentials, we choose the parameters of a DF for the Galaxy's stars such that the DF correctly predicts the distributions of the three principal velocity components in each of eight spatial bins around the Sun. The selected DF then predicts the vertical density profile of stars in the solar cylinder. If the mass model assigns most mass to the disc, the predicted stellar profile decreases very steeply with distance from the plane because the gravitational potential has a deep minimum at $z = 0$. Conversely, if the mass model assigns little mass to the disc, the potential's minimum at $z = 0$ is shallow and the predicted stellar density declines slowly with distance from the plane. We identify the true potential by requiring that the predicted density profile is consistent with density profiles inferred from star counts.

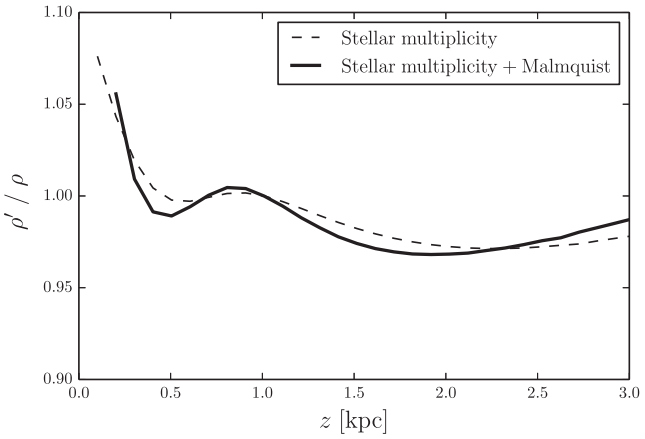

Figure 1. Ratio of the artificially biased vertical mass density profile ρ' to the original profile ρ as a function of height above the Galactic plane z.

In the next subsection, we explain how we selected candidate mass distributions, and in Section 3.2 we present our multiparameter DF.

3.1 The mass model

It is obviously sensible to take the fullest possible advantage of existing constraints on the Galaxy's mass distribution when selecting mass models. Indeed, although the RAVE data dramatically tighten constraints on the vertical distribution of matter, they are not well suited to constraining the radial distribution of matter – estimates of the circular speed and the dynamics of halo tracers and satellite galaxies are much better suited to that task. Here, we use a methodology similar to that employed by Caldwell & Ostriker (1981), Dehnen & Binney (1998) and McMillan (2011) to identify a few-parameter family of mass models that can be confronted with the RAVE data.

Our mass models have five components: a gas disc, a thin disc, a thick disc, a flattened bulge and a dark halo. Since the stellar halo has negligible mass, we do not explicitly include it in the mass model; its tiny mass is negligible from a dynamical point of view and can be considered subsumed within the dark halo. It is, however, important when we consider the phase space distribution of stars and we therefore include it in our stellar DF in Section 3.2. For the density laws of the disc components, we have

$$\rho(R, z) = \frac{\Sigma_0}{2z_{\rm d}} \exp\left[-\left(\frac{R}{R_{\rm d}} + \frac{|z|}{z_{\rm d}} + \frac{R_{\rm hole}}{R}\right)\right], \quad (8)$$

where R and z are the coordinates in a Galactocentric cylindrical coordinate system and Σ_0, $R_{\rm d}$, $z_{\rm d}$ and $R_{\rm hole}$ are parameters. A non-zero parameter $R_{\rm hole}$ creates a central cavity in the disc. This is used to model the gas disc while for the other two discs it is set to zero. We further fix the fraction of the local baryonic surface density contributed by the gas disc to 25 per cent. The other fixed parameters for this component can be found in Table 1.

Downloaded from https://academic.oup.com/mnras/article-abstract/445/3/3133/1052064
by University of Hull user
on 29 June 2018

Table 1. Parameters that are fixed in our Galaxy mass model.

Gas disc	
$\Sigma_g(R_0)$	$(\Sigma_{\rm thin}(R_0) + \Sigma_{\rm thick}(R_0))/3$
$R_{\rm d,g}$	$2R_{\rm d,\,thin}$
$z_{\rm d,g}$ [kpc]	0.04
$R_{\rm hole,g}$ [kpc]	4
Bulge	
$\rho_{0,\rm b}$ [$M_\odot$ kpc^{-3}]	9.49×10^{10}
$q_{\rm b}$	0.5
$\gamma_{\rm b}$	0
$\beta_{\rm b}$	1.8
$r_{0,\rm b}$ [kpc]	0.075
$r_{\rm cut,b}$ [kpc]	2.1
Dark halo	
$q_{\rm dm}$	1
$\gamma_{\rm dm}$	1
$\beta_{\rm dm}$	3
$r_{\rm cut,dm}$ [kpc]	10^5

The density distributions of the dark halo and the bulge components are

$$\rho(R,z) = \frac{\rho_0}{m^\gamma(1+m)^{\beta-\gamma}} \exp[-(mr_0/r_{\rm cut})^2], \tag{9}$$

where

$$m(R,z) = \sqrt{(R/r_0)^2 + (z/qr_0)^2}. \tag{10}$$

Here, ρ_0 sets the density scale, r_0 is a scale radius, and the parameter q is the axis ratio of the isodensity surfaces. The exponents γ and β control the inner and outer radial slopes of the radial density profile.

For our standard model, we adopt a spherical NFW model (Navarro, Frenk & White 1996) ($q = 1$, $\alpha = 1$, $\beta = 3$, $r_{\rm cut} \simeq \infty$) for the dark halo. In Section 4.2, we also consider flattened halo configurations.

The bulge model is not varied in the course of our model fitting process, because we use no data that might constrain its parameters. Following McMillan (2011), we use a model similar to that constructed by Bissantz & Gerhard (2002). It has an axis ratio $q = 0.5$ and extends to $r_{\rm cut} = 2.1$ kpc: Table 1 lists the other parameters of the bulge.

Since the thin and the thick disc density laws have three free parameters each (Σ_0, $R_{\rm d}$, $z_{\rm d}$) and the dark halo has two free parameters (ρ_0, r_0), our mass model has eight parameters. Since our constraints are not suited to fixing differing scale radii for the two discs, we reduce the number of free parameters to seven by setting $R_{\rm d,\,thick} = R_{\rm d,\,thin}$. We then use the constraints from the literature listed in Section 2 to fix all remaining parameters except the local dark matter density, $\rho_{\rm dm,\odot}$, the scaleheights $z_{\rm thn}$ and $z_{\rm thk}$ of the thin and thick discs, and the parameter $f_{\rm thk}$, which determines the fraction $(1 + f_{\rm thk}^{-1})^{-1}$ of the local stellar mass density that is contributed by the thick disc. The approach closely follows that of McMillan (2011) except that we use the AMOEBA algorithm (Press et al. 2007) to find the parameter set with maximum likelihood instead of evaluating the full posterior via Markov Chain Monte Carlo (MCMC) as in McMillan (2011). Figs 2 and 3 illustrate a typical quality of fit that we achieve for the terminal velocities and the maser data.

The three parameters, $z_{\rm thn}$, $z_{\rm thk}$ and $f_{\rm thk}$ are finally fixed using the RAVE data and the stellar DF, which we describe in the next subsection.

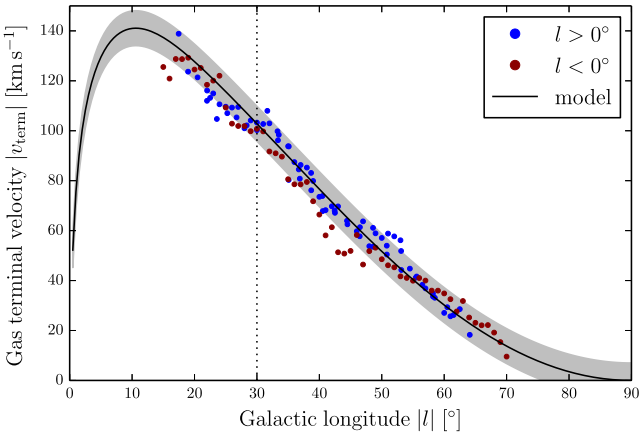

Figure 2. Comparison of the measured terminal velocities and the prediction by one of our mass models (solid black line). The grey shaded area illustrates the velocity dispersion of 7 km s^{-1} that we assumed. Measurements left of the dotted vertical line were not included for the fit. This particular model has the parameters given in Table 2, but the same quality of the fit is achieved for all reasonable choices for $\rho_{\rm dm,\odot}$ and the parameters for the vertical structure of the disc.

3.2 DF for the discs

Following Binney (2010a), we assume that the DFs of the discs can be well approximated by analytic functions of the three action integrals J_i. We use the 'Stäckel Fudge' introduced by Binney (2012a) to evaluate the J_i given phase-space coordinates $(\boldsymbol{x}, \boldsymbol{v})$. (Details of some technical improvements are given in Binney 2014.)

Our DFs are built up out of 'quasi-isothermal' components. The DF of such a component is

$$f(J_r, J_z, L_z) = f_{\sigma_r}(J_r, L_z) f_{\sigma_z}(J_z, L_z), \tag{11}$$

where f_{σ_r} and f_{σ_z} are defined to be

$$f_{\sigma_r}(J_r, L_z) \equiv \frac{\Omega\Sigma}{\pi\sigma_r^2\kappa}[1 + \tanh(L_z/L_0)]{\rm e}^{-\kappa J_r/\sigma_r^2} \tag{12}$$

and

$$f_{\sigma_z}(J_z, L_z) \equiv \frac{\nu}{2\pi\sigma_z^2}\,{\rm e}^{-\nu J_z/\sigma_z^2}. \tag{13}$$

Here, $\Omega(L_z)$, $\kappa(L_z)$ and $\nu(L_z)$ are, respectively, the circular, radial and vertical epicycle frequencies of the circular orbit with angular momentum L_z, while

$$\Sigma(L_z) = \Sigma_0 {\rm e}^{-R_{\rm c}/R_{\rm d}}, \tag{14}$$

where $R_{\rm c}(L_z)$ is the radius of the circular orbit, determines the surface density of the disc: to a moderate approximation this surface density can be obtained by using for L_z in equation (14) the angular momentum $L_z(R)$ of the circular orbit with radius R. The functions $\sigma_r(L_z)$ and $\sigma_z(L_z)$ control the radial and vertical velocity dispersions in the disc and are approximately equal to them at $R_{\rm c}$. Given that the scaleheights of galactic discs do not vary strongly with radius (van der Kruit & Searle 1981), these quantities must increase inwards. We adopt the dependence on L_z

$$\sigma_r(L_z) = \sigma_{r0}\,{\rm e}^{(R_0-R_{\rm c})/R_{\sigma,r}}$$

$$\sigma_z(L_z) = \sigma_{z0}\,{\rm e}^{(R_0-R_{\rm c})/R_{\sigma,z}}, \tag{15}$$

so the radial scalelengths on which the velocity dispersions decline are $R_{\sigma,i}$. Our expectation is that $R_{\sigma,\,i} \sim 2R_{\rm d}$.

Downloaded from https://academic.oup.com/mnras/article-abstract/445/3/3133/1052064
by University of Hull user
on 29 June 2018

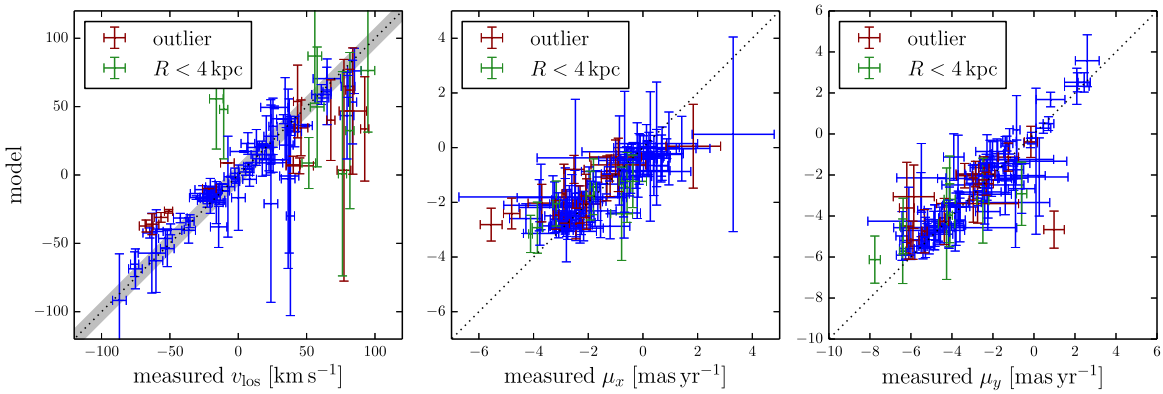

Figure 3. Comparison of the maser measurements by Reid et al. (2014) with our model predictions. The vertical error bars show the uncertainties arising from the uncertainties in the parallax estimations. In the leftmost panel, the grey shaded area illustrates the velocity dispersion of 7 km s^{-1} that we assumed. In the middle and rightmost panels, this velocity dispersion is already included in the vertical error bars because for proper motions this uncertainty is dependent on the individual distances of the masers. The sources plotted in red were considered outliers by Reid et al. (2014) and those closer than 4 kpc to the GC were excluded from the fit.

In equation (12), the factor containing tanh serves to eliminate retrograde stars; the value of L_0 controls the radius within which significant numbers of retrograde stars are found, and should be no larger than the circular angular momentum at the half-light radius of the bulge. Provided this condition is satisfied, the results for the extended solar neighbourhood presented here are essentially independent of L_0.

We take the DF of the thick disc to be a single pseudo-isothermal. The thin disc is treated as a superposition of the cohorts of stars that have age τ for ages that vary from zero up to the age $\tau_{\rm max} \simeq 10$ Gyr of the thin disc. We take the DF of each such cohort to be a pseudo-isothermal with velocity-dispersion parameters σ_r and σ_z that depend on age as well as on L_z. Specifically, from Aumer & Binney (2009) we adopt

$$\sigma_r(L_z,\tau) = \sigma_{r0}\left(\frac{\tau+\tau_1}{\tau_{\rm m}+\tau_1}\right)^{\beta} {\rm e}^{(R_0-R_{\rm c})/R_{\sigma,r}}$$

$$\sigma_z(L_z,\tau) = \sigma_{z0}\left(\frac{\tau+\tau_1}{\tau_{\rm m}+\tau_1}\right)^{\beta} {\rm e}^{(R_0-R_{\rm c})/R_{\sigma,z}}. \quad (16)$$

Here, σ_{z0} is the approximate vertical velocity dispersion of local stars at age $\tau_{\rm m} \simeq 10$ Gyr, τ_1 sets velocity dispersion at birth, and $\beta \simeq 0.33$ is an index that determines how the velocity dispersions grow with age. We further assume that the star formation rate in the thin disc has decreased exponentially with time, with characteristic time-scale t_0, so the thin-disc DF is

$$f_{\rm thn}(J_r,J_z,L_z) = \frac{\int_0^{\tau_{\rm m}} {\rm d}\tau\, {\rm e}^{\tau/t_0} f_{\sigma_r}(J_r,L_z) f_{\sigma_z}(J_z,L_z)}{t_0({\rm e}^{\tau_{\rm m}/t_0}-1)}, \quad (17)$$

where σ_r and σ_z depend on L_z and τ through equation (16). We set the normalizing constant Σ_0 that appears in equation (14) to be the same for both discs and use for the complete DF

$$f_{\rm disc}(J_r,J_z,L_z) = f_{\rm thn}(J_r,J_z,L_z) + F_{\rm thk} f_{\rm thk}(J_r,J_z,L_z), \quad (18)$$

where $F_{\rm thk}$ is a parameter that controls the fraction $(1+F_{\rm thk}^{-1})^{-1}$ of stars that belong to the thick disc.[2]

[2] Note that $F_{\rm thk}$ is the ratio of the total masses of the thick and the thin discs, while the parameter $f_{\rm thk}$ used for the mass model is the ratio of the local mass densities of the two discs. Hence, the two parameters are intimately related but not the same.

The DFs of the thin and thick discs each involve five important parameters, σ_{r0}, σ_{z0}, $R_{\rm d}$, $R_{\sigma,r}$ and $R_{\sigma,z}$. The DF of the thin disc involves four further parameters, τ_1, $\tau_{\rm m}$, β and t_0, but we shall not explore the impact of changing these here because we do not consider data that permit discrimination between stars of different ages. Therefore following Aumer & Binney (2009), we adopt throughout $\tau_1 = 0.01$ Gyr, $\tau_{\rm m} = 10$ Gyr, $\beta = 0.33$ and $t_0 = 8$ Gyr.

3.3 DF of the stellar halo

Due to the magnitude limits of RAVE, most of its stars belong to the thin and thick discs. The sample does, however, contain a small but non-negligible population of halo stars, which are identifiable by their low or even negative values of the azimuthal velocity V_ϕ (Piffl et al. 2014). We have added to the DF a component for the stellar halo to prevent the fitting routine distorting the thick disc in an attempt to account for the presence in the sample of halo stars.

The density of the stellar halo is generally thought to follow a power law in Galactocentric radius, i.e. $\rho_{\rm halo} \propto r^{-\alpha}$, with the power-law index $\alpha \simeq 3.5$ (e.g. Binney & Merrifield 1998, section 10.5.2). We can model such a configuration using the following form of the DF (Posti et al., in preparation)

$$f_{\rm halo}(J_r,J_z,L_z) = \left(\frac{h(L_{\rm c0})}{h(\boldsymbol{J})}\right)^{\alpha}, \quad (19)$$

where $h(\boldsymbol{J})$ is a homogeneous function of degree one [i.e. $h(\beta\boldsymbol{J}) = \beta h(\boldsymbol{J})$], and $L_{\rm c0}$ is the angular momentum of a circular orbit of radius R_0. When the circular speed is independent of radius, the density generated by the DF (19) declines with radius as $r^{-\alpha}$, so we adopt $\alpha = 3.5$. Our choice

$$h(\boldsymbol{J}) = J_r + \frac{\Omega_z}{\Omega_r} J_z + \frac{\Omega_\phi}{\Omega_r}|L_z|, \quad (20)$$

where $\Omega_i(\boldsymbol{J})$ are the characteristic frequencies of the orbit with actions $\boldsymbol{J}$, ensures that in a spherical potential the halo would be approximately spherical. Since the Galaxy's potential is somewhat flattened, our halo will be slightly flattened too. The RAVE data alone are not well suited to constraining the stellar halo, so we defer this exercise to a later paper. We include the stellar halo only in order to prevent distortion of the thick disc that is fitted to the data. Our complete total DF is

$$f(J_r,J_z,L_z) = f_{\rm disc}(J_r,J_z,L_z) + F_{\rm halo} f_{\rm halo}(J_r,J_z,L_z). \quad (21)$$

Downloaded from https://academic.oup.com/mnras/article-abstract/445/3/3133/1052064
by University of Hull user
on 29 June 2018

3.4 Model–RAVE comparison

RAVE, like any spectroscopic survey, has a non-trivial selection function: potential targets were divided into bands by apparent magnitude and then the spectrograph's fibres were allocated to as many stars as possible in a given band with the exposure time being band-specific. From the resulting spectra the pipeline extracts acceptable stellar parameters with a probability that to some extent depends on metallicity. Hence, the probability that a given star enters the final catalogue – the selection function – depends on the star's apparent magnitude, location and metallicity. These probabilities will be derived and discussed in a forthcoming paper (Piffl et al., in preparation), and we proceed here without using these probabilities.

Of the above-mentioned selection criteria, only the metallicity is – via the birth time and place of a star – correlated with the stellar velocities. Fortunately, the great majority of spectra yield stellar parameters, so the dependence of the selection function on metallicity is weak. If we neglect this weak dependence, the selection function is independent of stellar velocity, so we can predict the velocity distribution $n(\boldsymbol{v}) = f(\boldsymbol{x}, \boldsymbol{v})/\rho(\boldsymbol{x})$ of the catalogued stars from a model's DF, $f(\boldsymbol{x}, \boldsymbol{v})$. It is interesting to ask to what extent the DF of the RAVE stars is constrained by the velocity distributions presented by Binney et al. (2014b). We focus on the velocity distributions of the giant stars ($\log g < 3.5$) which provide wider spatial coverage than the dwarf stars. In Section 5, we will compare the RAVE data for hot dwarf stars ($\log g > 3.5$ and $T_{\rm eff} > 6000$ K) with the predictions made by the most successful of the DFs we obtain by fitting the giants.

We define eight spatial bins in the (R, z) plane. Four bins for stars inside the solar cylinder with $R_0 - 1\,{\rm kpc} < R < R_0$ and $|z|$ in [0,0.3],[0.3,0.6],[0.6,1.0] or [1,1.5] kpc. The other four bins cover the same z ranges but cover the regions 1 kpc outside the solar cylinder, i.e. $R_0 < R < R_0 + 1\,{\rm kpc}$. After sorting the stars into these bins, we compute the velocity distributions predicted by the DF at the mean (R, z) positions (barycentre) of the stars in each bin. For each bin, we have a histogram for each component of velocity, so we accumulate χ^2 from 24 histograms. Throughout this work, we compute velocities in the coordinate system that Binney et al. (2014b) found to be closely aligned with the velocity ellipsoid throughout the extended solar neighbourhood – this system is quite closely aligned with spherical coordinates. We denote the velocity component along the long axis of the velocity ellipsoid – pointing more or less towards the GC – with V_1, the azimuthal component with V_ϕ, and the remaining component with V_3 which is close to the latitudinal direction (cf. also Bond et al. 2010).

The resulting model distributions cannot be directly compared to the observed distributions, because the latter are widened by errors in the velocity and parallax estimates. We fold the model distributions with the average velocity uncertainties of the bin's stars to obtain $N_{\rm bary}(V_i)$. The distortions arising from the parallax error are less straightforward to introduce: following Binney et al. (2014b), we create a Monte Carlo realization of a given DF by randomly assigning to each star in our RAVE sample a new 'true' distance according to its (sometimes multimodal) distance pdf, and a new 'true' velocity according to the model velocity distribution at this position. With these new phase-space coordinates, we compute new observed line-of-sight velocities and proper motions. These are finally equipped with random observational errors. Using the original catalogue distances, we then compute new realistically distorted velocity distributions, $N_{\rm MC}(V_i)$, based on the DF that can be compared directly to the original RAVE distributions in a number of spatial bins. We minimize the Poisson noise in $N_{\rm MC}(V_i)$ by choosing 100 new velocities for each star. This procedure is computationally expensive and the distortions vary only weakly for reasonable choices of the DF parameters. To speed up the process, we store the ratio $N_{\rm bary}(V_i)/N_{\rm MC}(V_i)$ for a DF that is already a good match of the RAVE data. Examples of these ratios are shown in the lower panels of Fig. 4 while the upper panels plot the actual distributions. The ratio is near unity in the core of the distribution but falls to <0.2 in the wings because distance errors scatter stars to high apparent velocities. These ratios are then used to correct all DF predictions before they are compared with the data.

This approach is far from perfect, because by comparing velocity histograms instead of assigning likelihoods to individual stars we lose the information encoded in the correlations between the velocity components. However, an approach based on computing likelihoods for the full phase-space distribution is currently computationally too expensive to allow for testing a large number of models.

With our approach and the RAVE giant sample, we can determine the values of the DF parameters to very high precision. UsingMCMC re-sampling, we find that the pseudo-velocity dispersions are

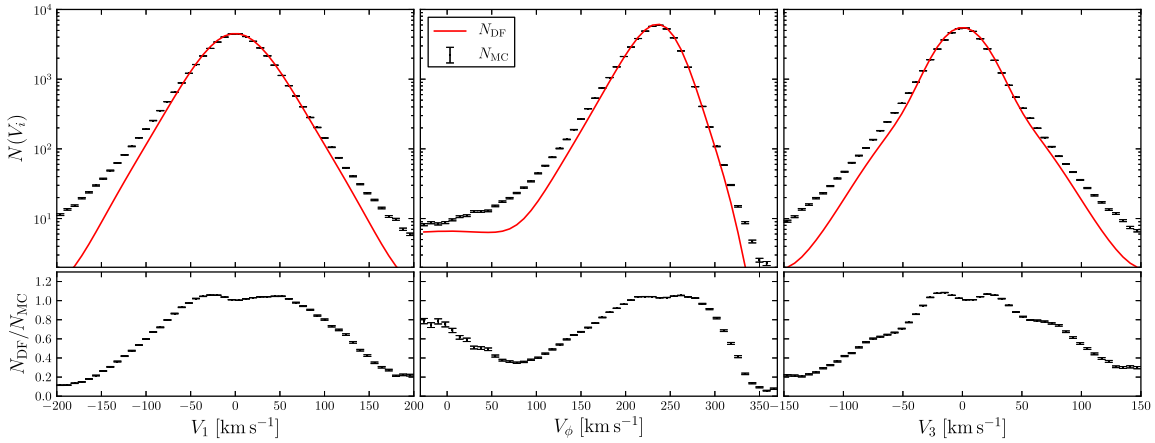

Figure 4. Distortion on the velocity distributions by uncertainties in the RAVE distances. The three upper panels are histograms of the three velocity components for stars with $R < R_0$ and $|z| < 0.3$ kpc. The solid red lines show the number of stars predicted by the DF at the barycentre of the bin, and the error bars show the numbers of stars selected by Monte Carlo re-sampling. For the latter we take the mean of 100 realizations. The lower panels show the value of the DF divided by the number of stars in the Monte Carlo sample.

Downloaded from https://academic.oup.com/mnras/article-abstract/445/3/3133/1052064
by University of Hull user
on 29 June 2018

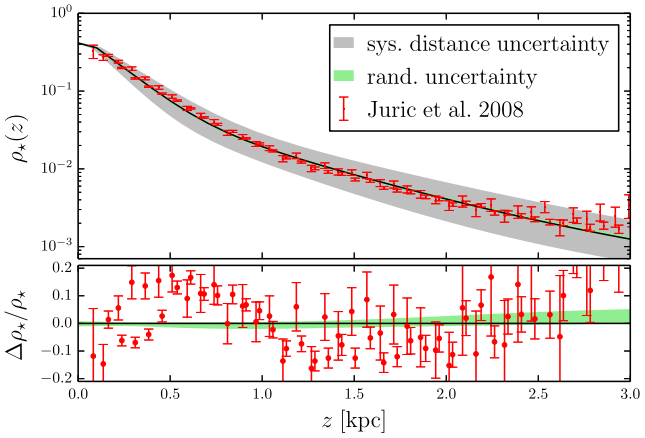

Figure 5. Vertical stellar density profile as predicted by the DF (upper panel) and relative random residuals (lower panel). The green shaded area shows the random variations introduced by the uncertainty of the DF parameters when fitted to the RAVE data. The measurements and uncertainties from J08 are also shown for comparison. The grey shaded area illustrates the uncertainty introduced by the uncertain distance scale of J08. Note that the model profiles were only constrained by stars with $|z| < 1.5$ kpc.

fixed to a fraction of a per cent, while the thick disc dispersion scalelengths and $F_{\rm thk}$ are fixed to ∼2 per cent. Only the stellar halo normalization has a relatively large uncertainty of $\lesssim 7$ per cent as is to be expected from the small number of halo stars in RAVE. Fig. 5 illustrates the resulting uncertainties on the vertical disc profile. Clearly the uncertainties on the J08 distance scale dominate the error budget by far.

3.5 Finding a pair

We now describe how we find what we call a 'self-consistent' mass model–DF pair that has a predefined value of the dark matter density at the position of the Sun, $\rho_{\rm dm,\odot}$, and is consistent with the kinematics the RAVE giants. With the ingredients outlined above we cannot construct a truly self-consistent model in the sense that both the collision-less Boltzmann equation and the Poisson equation are fulfilled as in Binney (2014), because we do not include the dark halo and the bulge in our DF. We call a mass model–DF pair 'self-consistent' if the mass distribution of the stellar disc implied by the DF is consistent with the mass distribution of the stellar disc assumed in the mass model.

In this spirit, we identify the disc scalelengths in the DF with the scalelengths in the mass model, and we equate in the DF and the mass model the parameters $F_{\rm thk}$ that determine the fraction of stars that belong to the thick disc.

It is a priori to be expected that the RAVE data do not strongly constrain the values of the scalelengths $R_{\sigma,r}$ and $R_{\sigma,z}$ of the velocity dispersions in the thin disc because, by virtue of the survey's avoidance of regions of low Galactic latitude b, radii R that differ materially from R_0 are only probed at high $|z|$, so radial and vertical gradients of the dispersions are hard to disentangle, especially as the thick disc dominates at high $|z|$. Experiments with the data confirm that the $R_{\sigma,i}$ of the thin disc are poorly constrained. In fact, if allowed to vary, their values tend to infinity, implying that the thin disc flares strongly, contrary to observation. We decided to fix the value of the $R_{\sigma,i,\rm thn}$ to 9 kpc which is 3–4 times the values of the scalelength the data imply for the mass model. We tested smaller and larger values of $R_{\sigma,i}$ for the thin disc and found no significant influence on our results.

With these assumptions our Galaxy model contains 4+7 free parameters: $\rho_{\rm dm,\odot} \equiv \rho_{\rm dm}(R_0, z_0)$, $z_{\rm d,\,thn}$, $z_{\rm d,\,thk}$ and $F_{\rm thk}$ for the mass model and $\sigma_{r0,\rm thn}$, $\sigma_{z0,\rm thn}$, $\sigma_{r0,\rm thk}$, $\sigma_{z0,\rm thk}$, $R_{\sigma,r\rm thk}$, $R_{\sigma,z\rm thk}$ and $F_{\rm halo}$ for the DF.

Given a mass model, it is computationally relatively cheap to adjust the parameters in the DF to optimize the fit between the predicted and observed velocity histograms. By contrast, any change in the mass model requires the relatively costly computation of new actions at a large number of points in phase space. Hence, we proceed as follows: for a trial mass model, we use AMOEBA minimization to choose the DF that provides the best fit to the observed velocity histograms. Next, holding constant $\rho_{\rm dm,\odot}$, we apply AMOEBA to adjust the mass model to optimize the fit between the vertical density profile of the stars predicted by the DF and assumed by the mass model. In this process, we keep the velocity-dispersion parameters of the DF fixed, with the result that the fit between the predicted and RAVE kinematics deteriorates, but fortunately only moderately even when the predicted stellar profile is materially altered. Once the stellar density profiles associated with the mass model and the DF have been brought to good agreement, the parameters of the DF are fine-tuned by another run of AMOEBA to re-optimize the fit between the predicted and observed kinematics on the spatially binned data, and then the mass model is readjusted to restore optimum agreement between the vertical density profiles.

The outcome of this procedure is a DF and a mass model that are consistent with one another as regards the spatial distribution of stars, and consistent with the observed kinematics of the RAVE stars. As $\rho_{\rm dm,\odot}$ is increased, the mass of the disc decreases to ensure that the constraints from the terminal velocities and proper motion of Sgr A* continue to be satisfied, and the vertical density profile of the model discs becomes steadily shallower. For a small range of values of $\rho_{\rm dm,\odot}$, the model's profile is consistent with the star counts. Fig. 6 shows this process in action: the black curves show the density profile predicted by the DF of the self-consistent mass model–DF pair found for the value of $\rho_{\rm dm,\odot}$ that is indicated by the numbers 8, 9, ... on each curve, where the units are $10^{-3}\,{\rm M}_\odot\ {\rm pc}^{-3}$.

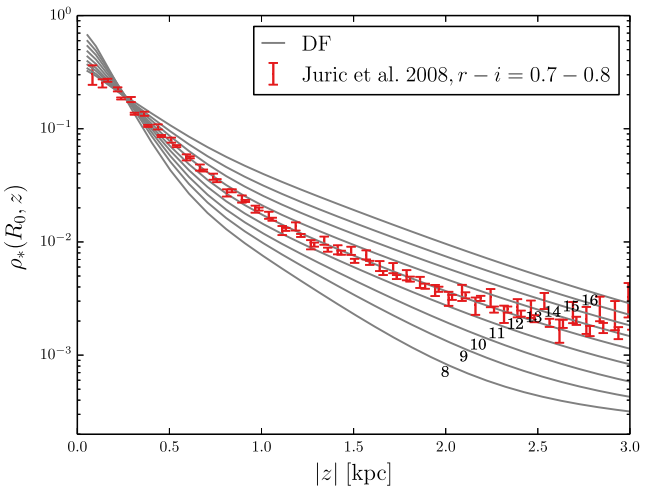

Figure 6. The full curves show the variation with $|z|$ of the number density of stars predicted by the best-fitting DF in mass models with various assumed values of $\rho_{\rm dm,\odot}$; each curve is labelled by $\rho_{\rm dm,\odot}$ in units of $10^{-3}\,{\rm M}_\odot\ {\rm pc}^{-3}$ and it can be shifted up or down at will. The red error bars show the number density of stars measured by J08.

Downloaded from https://academic.oup.com/mnras/article-abstract/445/3/3133/1052064
by University of Hull user
on 29 June 2018

4 RESULTS

The red points in Fig. 7 show χ^2 for the fit provided by each mass model–DF pair to the J08 data; the red dashed curve shows the best-fitting parabola through these points. Its minimum lies at $\rho_{\mathrm{dm},\odot} = 0.012\,62\,\mathrm{M}_\odot\ \mathrm{pc}^{-3}$ and its curvature implies a remarkably small uncertainty, ∼0.4 per cent. This is just the statistical uncertainty from the comparison to the observational profiles and should *not* be used, because – as we will show below – the systematic uncertainties are much larger. The DF parameters for the best-fitting model are given in Table 2.

Fig. 8 shows as a heavy black line the stellar density profile provided by the mass model–DF pair for local dark matter density $0.012\,\mathrm{M}_\odot\ \mathrm{pc}^{-3}$. The fit to the red data points, which show the star-count data from J08, is excellent both below and above the Galactic plane. The dashed grey lines in Fig. 8 show the densities

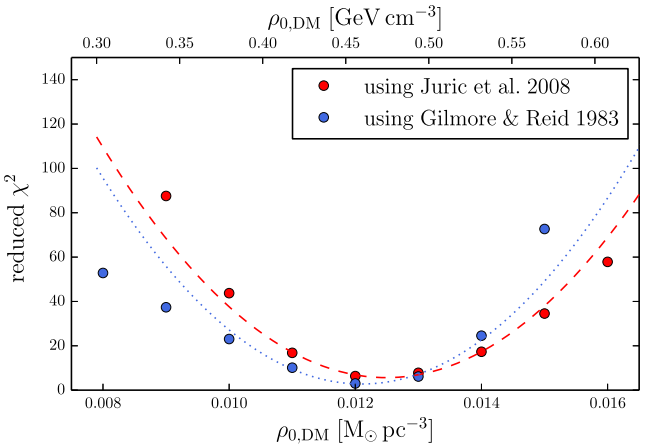

Figure 7. Red dots: reduced χ^2 distance between the vertical stellar mass profile predicted by the DF and the observational profiles by J08 as a function of the local density of a spherical dark matter halo. Blue dots show the reduced χ^2 distance from the density profile of Gilmore & Reid (1983). The red and blue dashed lines are parabolas fitted to the red/blue dots.

Table 2. Best-fitting parameters.

Model potential parameters		
$\Sigma_{0,\mathrm{thin}}$	570.7	$\mathrm{M}_\odot\ \mathrm{pc}^{-2}$
$\Sigma_{0,\mathrm{thick}}$	251.0	$\mathrm{M}_\odot\ \mathrm{pc}^{-2}$
R_d	2.68	kpc
$z_{\mathrm{d,thin}}$	0.20	kpc
$z_{\mathrm{d,thick}}$	0.70	kpc
$\Sigma_{0,\mathrm{gas}}$	94.5	$\mathrm{M}_\odot\ \mathrm{pc}^{-2}$
$R_{\mathrm{d,gas}}$	5.36	kpc
$\rho_{0,\mathrm{dm}}$	0.018 16	$\mathrm{M}_\odot\ \mathrm{pc}^{-3}$
$r_{0,\mathrm{dm}}$	14.4	kpc
DF parameters		
$\sigma_{r,\mathrm{thin}}$	34.0	$\mathrm{km\,s}^{-1}$
$\sigma_{z,\mathrm{thin}}$	25.1	$\mathrm{km\,s}^{-1}$
$R_{\sigma,r,\mathrm{thin}}$	9.0	kpc
$R_{\sigma,z,\mathrm{thin}}$	9.0	kpc
$\sigma_{r,\mathrm{thick}}$	50.6	$\mathrm{km\,s}^{-1}$
$\sigma_{z,\mathrm{thick}}$	49.1	$\mathrm{km\,s}^{-1}$
$R_{\sigma,r,\mathrm{thick}}$	13.0	kpc
$R_{\sigma,z,\mathrm{thick}}$	4.2	kpc
F_thick	0.447	
F_halo	0.026	

contributed by the thin and thick stellar discs of the mass model, while the dotted black curves show the densities yielded by the DF for the thin and thick discs and the stellar halo. At $z = 0$ the dashed curves from the mass model are unrealistically cusped on account of our assumption of naive double-exponential discs. Otherwise the agreement between the densities provided for the thick disc between the mass model and the DF is perfect. The agreement between the curves for the thin disc is nearly perfect within ∼1.5 scaleheights of the plane, but at greater heights, where the thick disc strongly dominates, the DF provides slightly lower density than the mass model. This discrepancy implies that the DF breaks the total stellar profile into thin- and thick-disc contributions in a slightly different way to the mass model. Since a real physical distinction between these components can only be made on the basis of age or chemistry (e.g. Binney & Merrifield 1998), the minor difference between the two thin-disc curves in Fig. 8 should not be considered significant at this stage.

The green error bars in Fig. 8 show the stellar densities inferred by Gilmore & Reid (1983) for stars with absolute visual magnitude M_V between 4 and 5 with an assumed vertical metallicity gradient of -0.3 dex kpc^{-1} (in their table 2). The blue dots in Fig. 7 show the χ^2 values we obtain when we adopt the Gilmore–Reid data points. They indicate a deeper minimum in χ^2 occurring at a smaller dark-halo density: $\rho_{\mathrm{dm},\odot} = 0.012\,00\,\mathrm{M}_\odot\ \mathrm{pc}^{-3}$.

4.1 Systematic uncertainties

The results presented above are based on a very sophisticated model that involves a number of assumptions and approximations. Deviations of the truth from these assumptions and approximations will introduce systematic errors into our results. We can assess the size of such systematic errors much more easily in some cases than in others. We have not assessed the errors arising from:

(i) the functional form of the mass model;
(ii) the functional form of the DF;
(iii) the age–velocity dispersion relation in the thin disc;
(iv) the adopted value of L_0 in disc DF: variation will affect the normalization of stellar halo;
(v) the power-law slope and quasi-isotropy of the stellar halo – we will investigate this in a future paper;
(vi) the solar motion w.r.t. the LSR.

The first two points include the approximation that the Galactic disc is smooth and axisymmetric, so the flows induced by spiral waves that have been detected by RAVE (Siebert et al. 2012; Williams et al. 2013) and in simulations (Debattista 2014; Faure, Siebert & Famaey 2014) are neglected.

We have investigated the sensitivity of our results to:

(i) R_0, which controls the circular speed: a value of $R_0 = 8$ kpc reduces $\rho_{\mathrm{dm},\odot}$ by 10 per cent.
(ii) The contribution of the gas disc to the local baryonic surface density. If we assume 33 per cent instead of our standard value of 25 per cent, we find slightly different structural parameters for the stellar discs, but our best-fitting value for $\rho_{\mathrm{dm},\odot}$ remains unchanged.
(iii) $R_{\sigma,i}$ for the thin disc: using $R_{\sigma,i} = 6$ kpc reduces $\rho_{\mathrm{dm},\odot}$ by <2 per cent.
(iv) The fact that $r_{0,\mathrm{dm}}$ changes with $\rho_{\mathrm{dm},\odot}$ on account of the halo constraints: setting $r_{0,\mathrm{dm}} = 20$ kpc increases $\rho_{\mathrm{dm},\odot}$ by 2 per cent.

Downloaded from https://academic.oup.com/mnras/article-abstract/445/3/3133/1052064
by University of Hull user
on 29 June 2018

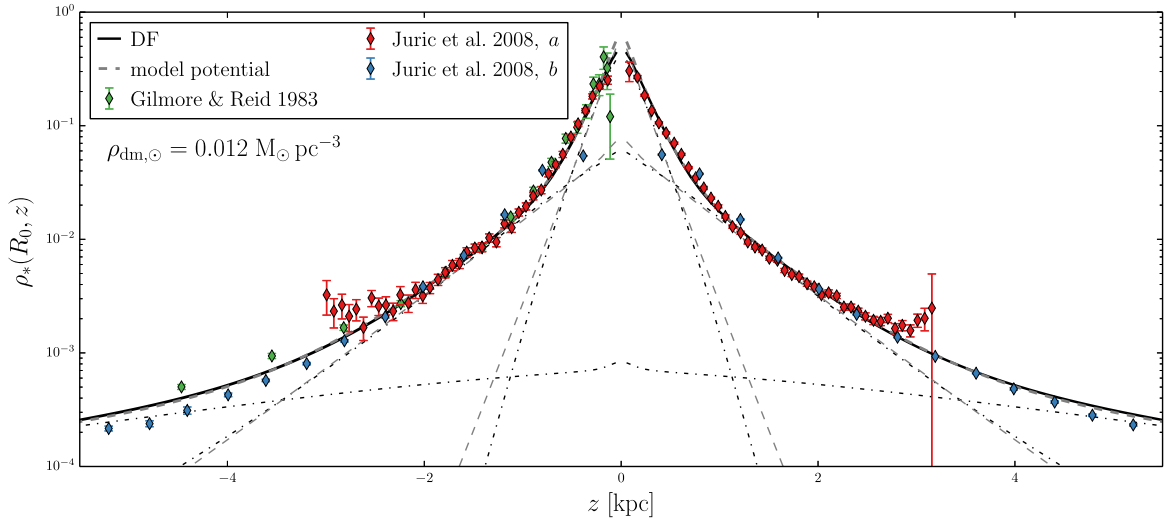

Figure 8. The full black curve shows the vertical density profile of the disc predicted by the DF for $\rho_{\mathrm{dm},\odot} = 0.012\,\mathrm{M}_\odot\ \mathrm{pc}^{-3}$; the mostly overlying dashed black curve shows the corresponding density profile in the mass model. The other dashed black lines show the profiles of the thin and thick discs in the mass model. The dotted curves show the corresponding predictions of the DF for both discs and the stellar halo (which has no explicit counterpart in the mass model). The red and blue error bars show the vertical profile measured by J08 for stars with $r - i \in [0.7, 0.8]$ ('a', red symbols) and with $r - i \in [0.15, 0.2]$ ('b', blue symbols). The latter was not used in the analysis and is shown only for illustrative purposes. The green error bars show the profile measured by Gilmore & Reid (1983).

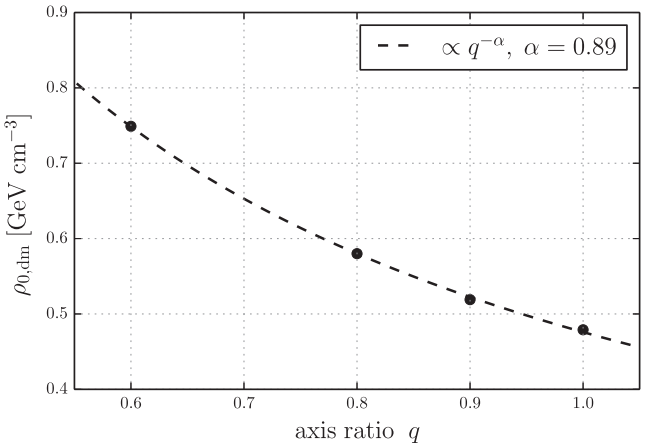

Figure 9. Best-fitting value for the local dark matter density $\rho_{\mathrm{dm},\odot}$ as a function of the assumed axis ratio q of the dark matter halo. A value of $q = 1$ implies a spherical halo, while smaller values lead to oblate configurations. The dashed black line shows a power law fitted using least-squares minimization.

(v) Equal scale radii for thin and thick disc: setting $R_{\mathrm{d,\,thick}}/R_{\mathrm{d,\,thin}} = 0.6$ (resulting in $R_{\mathrm{d,\,thick}} \simeq 2\,\mathrm{kpc}$ and $R_{\mathrm{d,\,thin}} \simeq 3.5\,\mathrm{kpc}$ similar to Bovy et al. 2012a), increase $\rho_{\mathrm{dm},\odot}$ by 4 per cent.

(vi) Flattening the dark halo: a flatter dark halo increases $\rho_{\mathrm{dm},\odot}$ significantly. See Fig. 9.

(vii) Systematic uncertainties in the distance scale of J08: if this distance scale is increased by a factor α, $\rho_{\mathrm{dm},\odot}$ proves to be almost proportional to α, with a 20 per cent increase in α causing $\rho_{\mathrm{dm},\odot}$ to increase by 8 per cent. A different value for the binary fraction has a very similar, but smaller, effect to a general change of the distance scale, and is hence also covered in this uncertainty. For a flattened dark matter halo with $q = 0.6$ the same test yielded a variation of 10 per cent.

The three most critical systematic uncertainties are therefore the axis ratio q of the dark halo, the solar distance to the GC and the distance scale used to construct the observational vertical stellar density profile. Simply adding in quadrature the uncertainties other than halo flattening listed above leads to a combined systematic uncertainty of ∼15 per cent. Combining this with the uncertainty associated with dark-halo flattening we arrive at our result

$$\rho_{\mathrm{dm},\odot} = \begin{cases} (0.48 \times q^{-\alpha})\mathrm{GeV\,cm}^{-3} \pm 15\,\mathrm{per\,cent} \\ (0.0126 \times q^{-\alpha})\mathrm{M}_\odot\,\mathrm{pc}^{-3} \pm 15\,\mathrm{per\,cent} \end{cases} \tag{22}$$

with $\alpha = 0.89$ and q the axis ratio of the dark halo. We remark that the given uncertainties are not statistically robust confidence intervals, but are estimates based on the above test runs. Because our kinematic data are restricted to $|z| < 1.5\,\mathrm{kpc}$, it is not possible for us to reliably single out a preferred value of q. For this, data at larger distances from the Galactic plane would be needed (cf. Fig. 10). In Section 6, we discuss this further.

Note that there is an additional potential source of uncertainty that we have not included in our estimate: Schönrich & Bergemann (2014) find hints that the common practice of assuming uncorrelated errors in the stellar parameters when deriving distance estimates leads to overconfident results. Hence, the parallax uncertainties reported by Binney et al. (2014a) might be underestimated. To test the possible influence, we doubled the individual parallax uncertainties (a worst case scenario) and repeated the fit. The best-fitting value for $\rho_{\mathrm{dm},\odot}$ increased by ∼7 per cent. A similar uncertainty is shared by all studies that use distances inferred from stellar parameters.

4.2 Flattening-independent results

The inverse dependence of $\rho_{\mathrm{dm},\odot}$ on q implies that for similar scale radii $r_{0,\mathrm{dm}}$ the mass of the dark matter halo within an oblate volume with axis ratio q is approximately independent of q. This is confirmed by Fig. 10 (upper panel), which shows the cumulative mass distribution as a function of elliptical radius.

The invariance of the dark matter mass profile can be qualitatively understood by the following consideration: flattening the dark halo

Downloaded from https://academic.oup.com/mnras/article-abstract/445/3/3133/1052064
by University of Hull user
on 29 June 2018

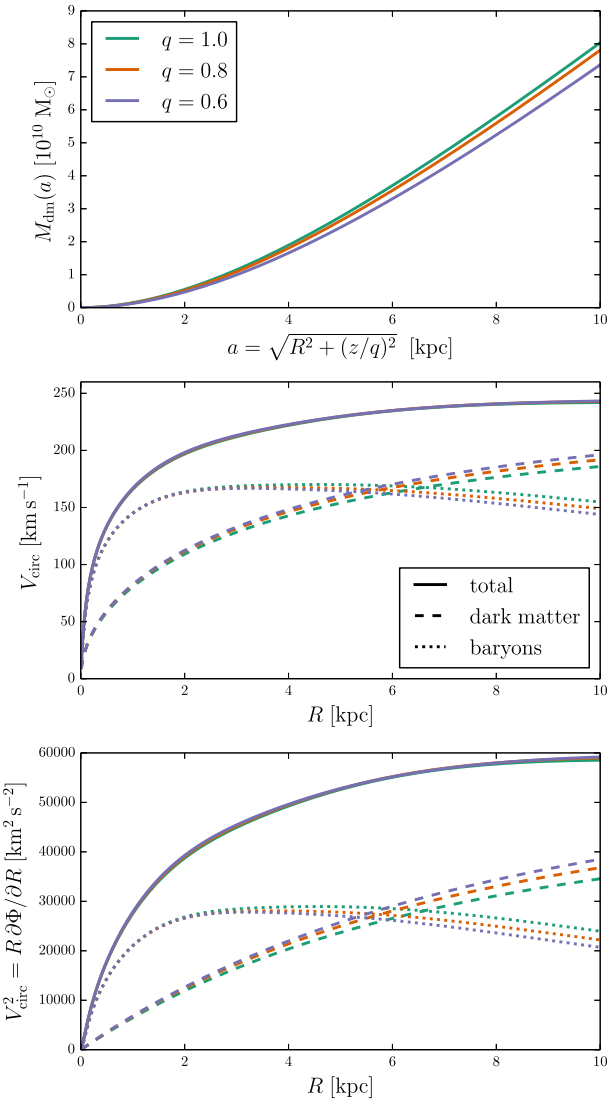

Figure 10. Upper panel: dark mass enclosed within the elliptical radius a for best-fitting models with three different axis ratios q: 0.6, 0.8 and 1. Middle panel: circular speed curves for the same models as in the upper panel. The dashed and dot–dashed lines show the circular speed curve generated by the dark matter halo and baryonic components alone. Bottom panel: same as the middle panel but showing squared circular speed as a function of R, which better illustrates the relative contributions of the dark matter and the baryons to the radial force at each radius.

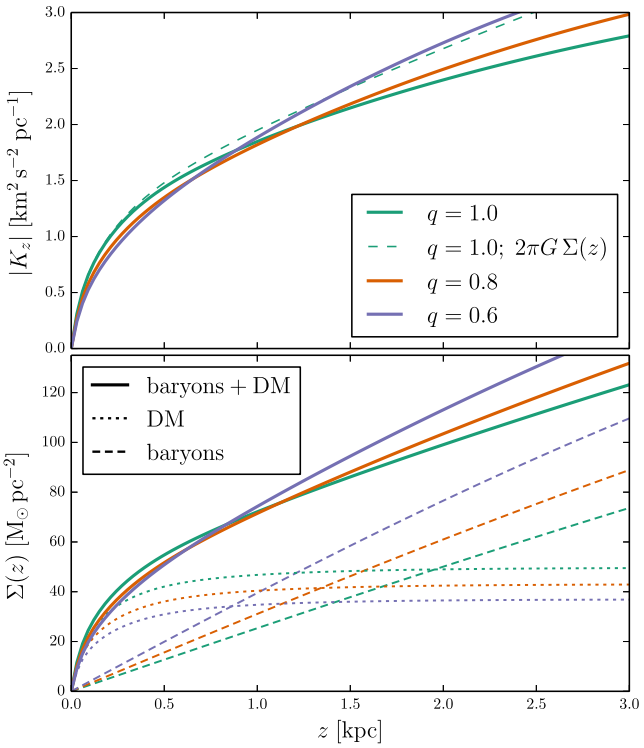

Figure 11. Upper panel: total vertical gravitational force as a function of distance from the Galactic plane for best-fitting models with three different dark-halo axis ratios q: 0.6, 0.8 and 1. The dashed turquoise line shows the K_z profile naively computed from the surface density profile using the simple conversion often used in the literature. At $|z| > 1$ kpc this diverges significantly from the true curve, namely the solid red line for the spherical dark halo. Lower panel: same as above, but this time the surface density $\Sigma(z)$ is shown: solid lines show the total surface density while dashed and the dot–dashed lines show the contributions of the dark halo and the Galactic disc.

at fixed local density reduces its mass and its contribution to the radial force, K_R. But – due to its still large thickness – its contribution to the vertical force K_z at low z remains almost constant or slightly grows. To restore the value of the circular speed at the Sun's location, we have to either increase the mass of the halo or that of the disc. However, filling the gap with disc material increases K_z and consequently compresses the vertical mass profile predicted by the DF. Thus the only possibility is to increase the mass of the halo and decrease the mass of the disc in order to keep K_z at the appropriate level. The upper panel of Fig. 10 illustrates that this increase does not fully balance the decrease from the initial flattening. The differences between the lines are much smaller than the variations coming from the systematic uncertainties. Taking the latter into account, we find the mass of dark matter interior to an ellipsoidal surface that goes through the solar annulus

$$M_{\rm dm}(a < R_0) = (6.0^{+1.35}_{-1.2}) \times 10^{10}\,{\rm M}_\odot$$

with $a = \sqrt{R^2 + (z/q)^2}$.

Interestingly, despite the fact that the enclosed dark mass is slightly decreasing with decreasing axis ratio, its contribution to the radial force increases. This is due to the enhanced gravitational pull of a flattened distribution and leads to a smaller baryonic mass required to sustain the rotation curve (middle and bottom panel of Fig. 10).

Fundamentally, the mass profiles are nearly independent of axis ratio because the observed kinematics determine the ability of stars to resist K_z, and the J08 density profile shows the extent to which they do resist K_z. Hence, K_z is narrowly constrained by the data independently of what mass distribution generates it. K_z is closely related to the surface density

$$\Sigma(z) = \int_{-z}^{z} {\rm d}z'\,\rho(R_0, z'). \tag{23}$$

Fig. 11 illustrates the z-dependences of these quantities for models with varying q. We see that there is a region around $z = 900$ pc where all profiles intersect. Taking into account the systematic uncertainties given above, we find

$$|K_z(z = 0.9\,{\rm kpc})| = (1.78 \pm 0.4)\,{\rm km^2\,s^{-2}\,pc^{-1}}.$$

Downloaded from https://academic.oup.com/mnras/article-abstract/445/3/3133/1052064
by University of Hull user
on 29 June 2018

For the surface density between ±900 pc, we find

$$\Sigma(z = 0.9\,\mathrm{kpc}) = (69 \pm 15)\,\mathrm{M}_\odot\,\mathrm{pc}^{-2}.$$

Below in Fig. 15, we set these measurements in context with estimates from the literature.

4.3 Other properties

We now give results for the model with a spherical dark halo. The best-fitting model has a virial mass[3] $M_{200} = (1.3 \pm 0.1) \times 10^{12}\,\mathrm{M}_\odot$. The above-mentioned systematic uncertainties translate into a <10 per cent uncertainty in the virial mass, but this does not encompass the uncertainty introduced by the assumed shape of the radial mass profile of the dark matter halo. For the models with flattened haloes, we find slightly increased virial masses of $1.4 \times 10^{12}\,\mathrm{M}_\odot$ and $1.6 \times 10^{12}\,\mathrm{M}_\odot$ for the axis ratios 0.8 and 0.6, respectively.

The total mass of the Galaxy's stellar disc is $(3.7 \pm 1.1) \times 10^{10}\,\mathrm{M}_\odot$. This is lower but not far from the canonical value of $5 \times 10^{10}\,\mathrm{M}_\odot$. It is within the range of 3.6 – $5.4 \times 10^{10}\,\mathrm{M}_\odot$ estimated by Flynn et al. (2006). Combining the stellar disc with the bulge and the gas disc, we arrive at a total baryonic mass $(5.6 \pm 1.6) \times 10^{10}\,\mathrm{M}_\odot$, or a baryon fraction (4.3 ± 0.6) per cent. This value is much lower than the cosmic baryon fraction of ∼16 per cent (Hinshaw et al. 2013; Planck Collaboration XVI 2013), once again illustrating the 'missing baryon problem' (e.g. Klypin et al. 1999). While this baryon fraction does not include the mass of the Galaxy's virial-temperature corona, the mass of the corona within ∼20 kpc of the GC is negligible (Marinacci et al. 2010); the missing baryons have to lie well outside the visible Galaxy in the circum- or intergalactic medium.

The thick disc contributes about 32 per cent of the disc's stellar mass which is lower than the 70 per cent found by J08. This result depends, however, on our decision to equate the radial scalelengths of the two discs. If the scalelength of the thick disc is assumed to be shorter, as found by Bovy et al. (2012a), the mass fraction in this component increases to ∼60 per cent. The better agreement with J08 is only apparent, however, because these authors found a *longer* scale radius for the thick disc.

Fig. 12 shows for several fairly successful spherical models the surface densities of the stellar and gaseous discs at R_0 (upper panel) and the ratio of the radial forces at R_0 from the baryons and dark matter (lower panel). The upper panel shows good agreement with the estimates of the baryonic surface densities derived from *Hipparcos* data by Flynn et al. (2006, coloured bands). The lower panel shows that equal contributions to the radial force are achieved for local dark matter densities $\rho_{\mathrm{dm},\odot}$ that are lower than our favoured value for a spherical halo, but still within the range encompassed by the systematic uncertainties, which is shaded grey. In our best-fitting model, the solar neighbourhood is mildly dark matter dominated with only 46 per cent of the radial force coming from gas and stars. Alternatively, we can look at the contribution of disc to the total rotation curve at 2.2 times the scale radius to check whether our disc is 'maximal' according to the definition of Sackett (1997). We find a ratio $V_{\mathrm{c,\,disc}}/V_{\mathrm{c,\,all}} = 0.63$ ($V_{\mathrm{c,\,baryons}}/V_{\mathrm{c,\,all}} = 0.72$) that is below the range of 0.75–0.95 for a maximal disc, but slightly above the typical range of 0.47 ± 0.08 (0.57 ± 0.07) for external spiral galaxies (Bershady et al. 2011; Martinsson et al. 2013). It is still lower than the value of 0.83 ± 0.04 found by Bovy & Rix (2013).

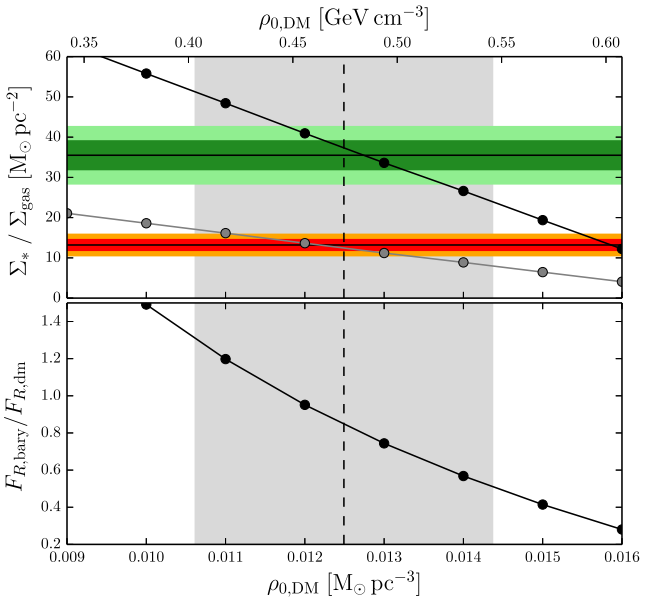

Figure 12. Upper panel: mass surface densities in our models for the stars (black points and lines) and gas (grey points and lines). The green and orange shaded area show the corresponding one/two sigma regions reported by Flynn et al. (2006). Lower panel: the ratio $F_{R,\mathrm{bary}}/F_{R,\mathrm{dm}}$ of the contributions to the radial force at R_0 from baryons and dark matter. In both panels, the grey shaded area illustrates the systematic uncertainties of $\rho_{\mathrm{dm},\odot}$ with the (interpolated) best-fitting value marked by the black dashed line. For this value, we have $F_{R,\mathrm{bary}}/F_{R,\mathrm{dm}} \sim 0.85$.

5 KINEMATICS

Here, we discuss the kinematic properties of our best-fitting model. The circular speed at the solar radius, $v_{\mathrm{c}}(R_0) = 240\,\mathrm{km\,s^{-1}}$ is largely the result of the adopted values of $R_0 = 8.3$ kpc, the proper motion of Sgr A*, and $\boldsymbol{v}_\odot$, the solar motion w.r.t. to the LSR. Our constraints for the mass model actually fix the ratio $v_{\mathrm{c}}(R_0)/R_0$ (McMillan 2011).

For the local escape speed $v_{\mathrm{esc}} = \sqrt{2\Phi(R_0)}$, we find a value of $613\,\mathrm{km\,s^{-1}}$. Piffl et al. (2014) recently found a lower value of $533^{+54}_{-41}\,\mathrm{km\,s^{-1}}$, but for this they used a modified definition of the escape speed as the minimum speed needed to reach $3R_{\mathrm{vir}}$. If we apply their definition to our model we find a value of $580\,\mathrm{km\,s^{-1}}$ which is still on the high side, but within their 90 per cent confidence interval. The uncertainties arising from the above-mentioned systematics on this value are of order 1 per cent. This comes mainly from our rather strong prior on the mass within 50 kpc and again does not cover the uncertainties in the dark matter profile at large radii.[4]

The data points in Fig. 13 show histograms for each principal velocity component and spatial bins defined by 7.3 kpc $< R < R_0$ and ranges in z that increase from bottom to top: the upper limits of the bins are at $z = 0.3$, 0.6, 1, 1.5 kpc and the coordinates of each bin's barycentre are given at the lower centre of each panel. The vertical scales of the plots are logarithmic and cover nearly three orders of magnitude in star density. The plotted velocity components V_1 and

[3] We define the virial mass as the mass interior to the radius R_{200} that contains a mean density of 200 times the critical density for a flat universe, ρ_{crit}.

[4] Because of this and also because of the focus of Piffl et al. (2014) on the fastest stars in the RAVE survey, which carry most of the information on the escape speed, we still consider their value as the more robust one.

Downloaded from https://academic.oup.com/mnras/article-abstract/445/3/3133/1052064
by University of Hull user
on 29 June 2018

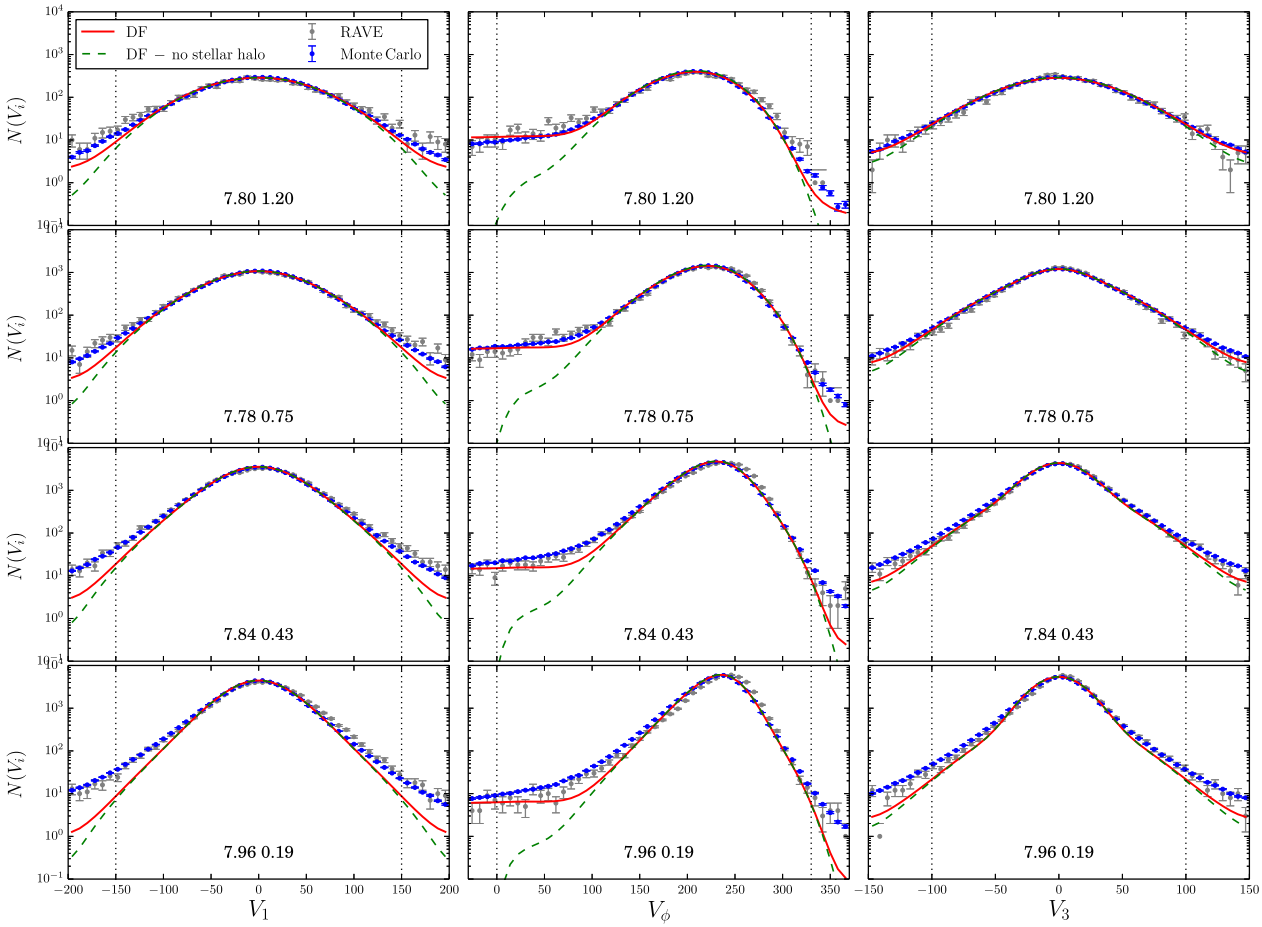

Figure 13. Velocity distributions in four spatial bins. In each panel, the numbers at the lower centre give the (R, z) coordinates of the bin's barycentre. The grey error bars show the RAVE data, while the green error bars show the mean of 10 Monte Carlo re-samples of our model with $\rho_{\mathrm{dm},\odot} = 0.012\,\mathrm{M}_\odot\ \mathrm{pc}^{-3}$, which is close to our best-fitting value. The vertical dotted lines show the boundaries of the velocity ranges over which χ^2 was computed. The full red curves show the predictions of the DF in the absence of distance errors, while the dashed lines show the corresponding predictions when the DF of the stellar halo is deleted.

V_3 are along directions $\boldsymbol{e}_1$ and $\boldsymbol{e}_2$ that lie very close to the radial and latitudinal directions, respectively, their precise directions being those determined by Binney et al. (2014b) to be the eigenvectors of the velocity dispersion tensor. The Poisson error on each data point is marked by the error bar and is in most cases insignificant. The grey data points represent the original RAVE data, while the green symbols show the mean of 100 Monte Carlo re-samplings using the mass model–DF pair with $\rho_{\mathrm{dm},\odot} = 0.012\,\mathrm{M}_\odot\ \mathrm{pc}^{-3}$, which is closest to our best-fitting value. Within the considered velocity ranges (bracketed by the vertical dashed lines in the panels), the fits to the data are good. For the V_ϕ-distributions, there is a systematic shift by approximately $5\,\mathrm{km\,s}^{-1}$. This shift is much smaller or even reversed for the spatial bins that lie beyond R_0, which suggests that it arises from spiral structure.

Far from the plane, the wings of the V_1 distributions are systematically underpredicted while there is a hint of an overprediction near the plane. A similar trend is apparent for the low-angular momentum stars in the V_ϕ distributions and this anomaly is also present in the histograms for bins that lie outside R_0. These trends suggest that the stellar halo density decreases less quickly with increasing $|z|$ than our model predicts, and hence that this component is *less* flattened than we have implicitly assumed by adopting the form (20) of the function h that appears in the halo DF. A definitive statement is, however, impossible, because the wings of the distribution are strongly affected by the uncertain distance estimates (and our modelling of this effect). Stars at greater heights from the Galactic plane, such as those in the *SEGUE* survey (Yanny et al. 2009) would yield a clearer picture.

5.1 Kinematics of hot dwarfs

We next look at the kinematics predicted for a different set of RAVE observations, namely hot dwarf stars. Stars in this group, defined by $\log g > 3.5$ dex and $T_{\mathrm{eff}} > 6000\,\mathrm{K}$, have the most precise distance estimates, but due to their lower luminosity they can be seen in a smaller volume than the giants. So we use spatial bins defined by smaller distances from the Galactic plane: we place the borders at $|z| = 0.15,\ 0.3,\ 0.45,\ 0.6\,\mathrm{kpc}$. Since these stars cannot be old, we assume their DF is given by the portion of the thin-disc DF for age below $5\,\mathrm{Gyr}$ ($=\tau_{\mathrm{m}}$). The green data points in Fig. 14 show the resulting Monte Carlo re-sampling of stellar distances and velocities, while the grey points show the RAVE data. The predicted and observed distributions agree well in their cores, but in their wings the RAVE data lie higher, especially in the case of V_1. The predicted V_ϕ distributions underpopulate the high-V_ϕ tails. Both phenomena are symptomatic of a model population that

Downloaded from https://academic.oup.com/mnras/article-abstract/445/3/3133/1052064
by University of Hull user
on 29 June 2018

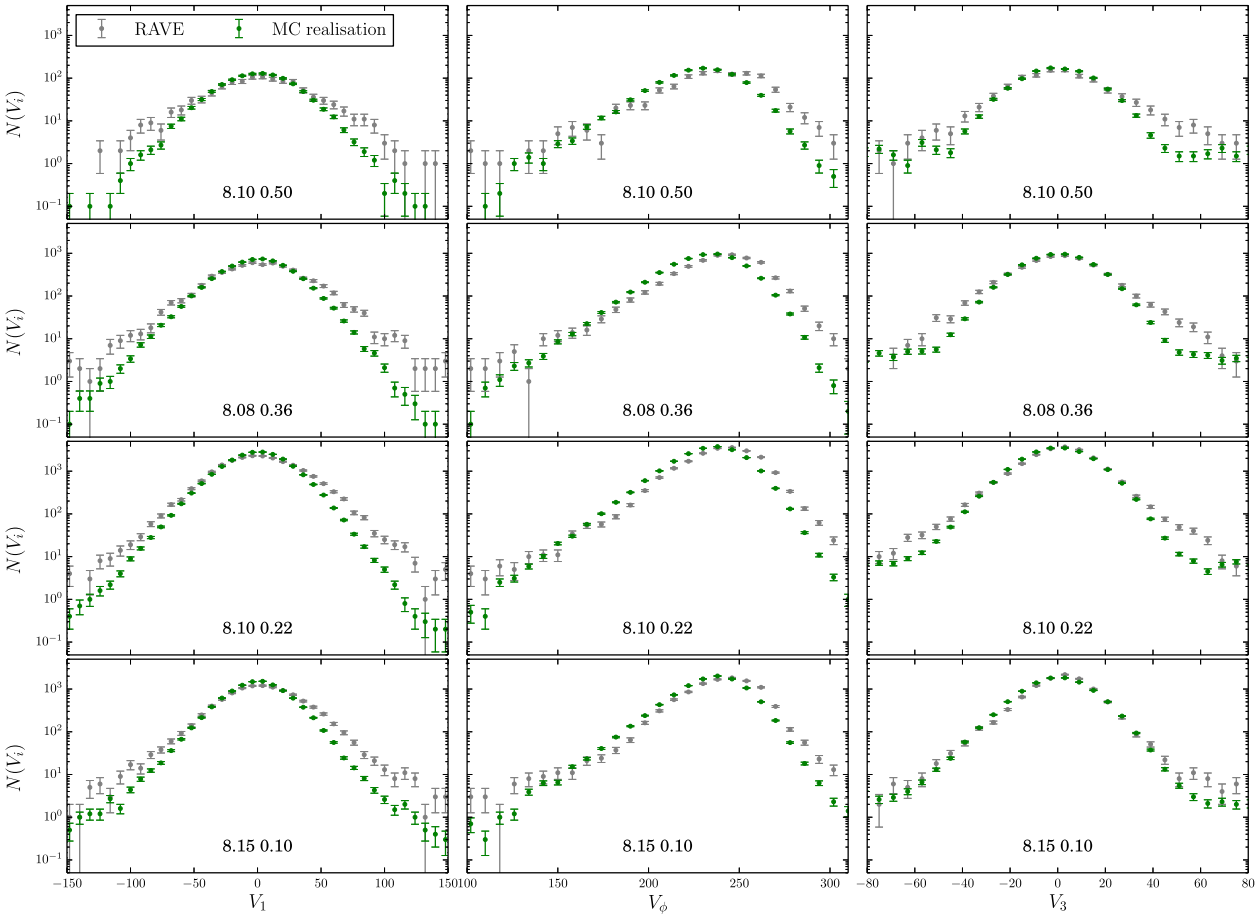

Figure 14. Velocity distributions of hot dwarfs in four spatial bins. These plots are similar to those in Fig. 13, but the borders of the bins are (from bottom to top) at $|z| = 0.15, 0.30, 0.45$ and 0.6 kpc. The (R, z) positions of the barycentres of the sub-samples are given in each panel. The grey error bars show the RAVE data while the green error bars show the mean of 10 Monte Carlo re-samples of the model with $\rho_{\mathrm{dm},\odot} = 0.012\,\mathrm{M}_\odot\ \mathrm{pc}^{-3}$, which is close to our best-fitting value.

has less random motion than the real one. It might be argued that 5 Gyr is an excessively young age to adopt for this population, which will contain stars with masses down to 1.1 $\mathrm{M}_\odot$ that live in excess of 7 Gyr. With an age cutoff of 7.5 Gyr improved fits to the V_1 distributions are obtained, but overall the velocity distributions remain deficient, and anyway the adopted age cutoff should match the mean lifetime of the population, not that of the longest-lived stars within it.

The discrepancies between theory and observation in Fig. 14 tie in with the DF's curve for the thin disc in Fig. 8 falling rather steeply at large $|z|$. It also ties in with a surprising result encountered by B12b when fitting DFs like those used here to the GCS: the thin-disc DF fully populated the wings of the U distribution of GCS stars with the result that when a thick-disc DF was added, using both the GCS velocities and the vertical density profile of Gilmore & Reid (1983), the implied radial velocity dispersion of the thick disc was lower than that of the old thin disc. Here, bins at large $|z|$ strongly influence the fitted DF, so the DF of the thick disc has sufficient in-plane dispersion to fill out the wings of these distributions. With our chosen functional form of the DF, the thick disc's DF then places enough stars in the bins near the plane to fill out the wings of these distributions. It follows that the thin-disc DF is then chosen such that it does not place additional, now unwanted, stars in the wings of the V_1 distributions at low $|z|$. Unfortunately, the RAVE distribution for hot dwarfs, which are surely thin-disc stars, shows that the thin disc *does* make a non-negligible contribution to the wings of the V_1 distribution.

The difficulty encountered here with the hot dwarfs and the difficulty encountered by B12b with the thick disc may both arise from an inappropriate choice for the functional dependences of the DF on J_r and J_z. These dependences are not motivated by any convincing physical arguments (but see Binney 2010b, for a relevant discussion), they are simply those provided by familiar analytic functions that have the right general properties. The superb statistics provided by the RAVE survey may oblige us to tweak these functions. This is, however, a topic for another paper.

6 DISCUSSION

We have built models of the Galaxy using the vast data set provided by the RAVE survey together with additional observations constraining the Galactic rotation curve and the stellar density profile above and below the Sun. In combination these measurements allowed us to disentangle the contributions to the local gravitational field of the baryonic and the dark matter and hence put tight constraints on the mass of the dark halo that lies interior to the Sun, and on the surface density of matter that lies within ∼0.9 kpc of the plane near the Sun. In order to compare our results to previous measurements in the literature one should keep in mind that

Downloaded from https://academic.oup.com/mnras/article-abstract/445/3/3133/1052064
by University of Hull user
on 29 June 2018

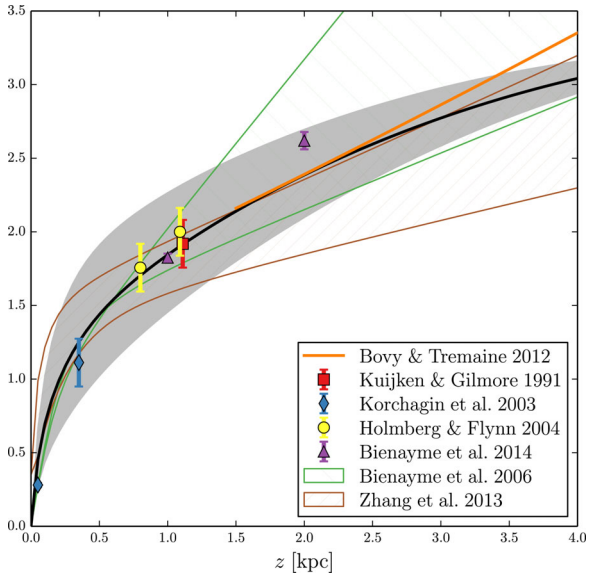

Figure 15. Vertical force law for our best-fitting model with a spherical dark halo (solid black line) and its systematic uncertainty (grey shaded area). The error bars and hatched regions show several other estimates from the literature. The estimate by Bovy & Tremaine (2012) was computed using their preferred parameters (dashed curve in their fig. 2).

our quoted uncertainties are not the statistical uncertainties which are negligible (<0.4 per cent), but originate purely from a conservative estimate of our systematic uncertainties. Similar systematic uncertainties are generally present in other studies.

A comprehensive review of estimates of the local dark matter density was recently published by Read (2014). Most of the more recent studies find lower values of $\rho_{\mathrm{dm},\odot}$ than our estimate of $0.0126\,\mathrm{M}_\odot\,\mathrm{pc}^{-3} \pm 15$ per cent for a spherical dark halo. Almost all previous studies rely on the assumption that the motions of stars near the Sun are separable into radial and vertical components. Recent examples of this approach are Bovy & Tremaine (2012, $0.008 \pm 0.003\,\mathrm{M}_\odot\,\mathrm{pc}^{-3}$) or Zhang et al. (2013, $0.0065 \pm 0.0023\,\mathrm{M}_\odot\,\mathrm{pc}^{-3}$). However, Garbari et al. (2012) showed by analysing mock data sets from *N*-body simulations that this can bias the results to lower values. They propose a new method that weakens this assumption and use this to re-analyse the data by Kuijken & Gilmore (1991). Both their estimate and their revised value $0.0087^{+0.007}_{-0.002}\,\mathrm{M}_\odot\,\mathrm{pc}^{-3}$ in Read (2014) are consistent with our results. Also most other recent studies that do not rely on the separability assumption find value for $\rho_{\mathrm{dm},\odot}$ that are in good agreement with our measurement (Salucci et al. 2010; Iocco et al. 2011; McMillan 2011; Nesti & Salucci 2013).

Parallel to this work, Bienaymé et al. (2014) used a sample of ∼4600 red clump stars from RAVE to measure the vertical force (see Fig. 15 below) and from a more classical approach concluded that the local dark matter density is $\rho_{\mathrm{dm},\odot} = 0.0143 \pm 0.0011\,\mathrm{M}_\odot\,\mathrm{pc}^{-3}$. Their results are very similar to the results of this study despite a radically different methodology, different distance estimates, and only a partial overlap of the stellar samples. In particular, they used stars at $|z| > 1.5$ kpc that were excluded for our study.

6.1 Surface density and vertical force

It is often assumed that once one has determined the vertical force K_z acting on stars at a certain height z above or below the Galactic plane, this can be trivially converted into the surface mass density between $\pm z$. It was already remarked before that this is a good approximation only for small $|z|$. A comparison of the dashed and solid red lines in the upper panel of Fig. 11 illustrates this once again (see also Bovy & Tremaine 2012). Previously, with sample sizes of hundreds or few thousand stars, the distinction could be generously ignored. With almost 200 000 stars, the statistical uncertainties become negligible and adopting $K_z = 2\pi G\Sigma$ introduces a significant bias. It is hence advisable not to confuse K_z and $2\pi G\Sigma$.

The full black curve in Fig. 15 shows the K_z profile of our best-fitting model, while the grey band shows our systematic uncertainty. Clearly these results are in excellent agreement with the data points, which show the estimates of Bovy & Tremaine (2012), Kuijken & Gilmore (1991), Korchagin et al. (2003), Holmberg & Flynn (2004), Bienaymé et al. (2006), Bienaymé et al. (2014) and Zhang et al. (2013). Note that uncertainties of these earlier studies are random errors, while our uncertainties from random errors are negligible.

Interestingly, the study by Bienaymé et al. (2014) extended the range of $|z|$ values probed to 2 kpc, so above the volume in which our stars reside. Their steep gradient between 1 and 2 kpc could be interpreted as indicating a flattened dark halo with axis ratio $q \lesssim 0.8$ (cf. the upper panel of Fig. 11). Their slightly higher value for $\rho_{\mathrm{dm},\odot}$ is consistent with this, as it requires q to be 0.79–0.94 to match our results.

Moni Bidin et al. (2012b) claimed that the kinematics of a sample of distant red giants from Moni Bidin, Carraro & Méndez (2012a) proves that $\rho_{\mathrm{dm},\odot}$ is negligible. However, Sanders (2012) showed that the velocity dispersion gradients reported by Moni Bidin et al. (2012a) were most likely too shallow by a factor 2–3 and their uncertainties severely underestimated. Bovy & Tremaine (2012) showed that the analysis in Moni Bidin et al. (2012b) is flawed, and from the data in Moni Bidin et al. (2012a) derived a value for $\rho_{\mathrm{dm},\odot}$ that is consistent with a significant dark halo. However, the errors on $\rho_{\mathrm{dm},\odot}$ given by Bovy & Tremaine are based on the erroneous errors in Moni Bidin et al. (2012a), and the use of realistic errors would probably prohibit any significant statement.

We nevertheless include the results of Bovy & Tremaine (2012) in Fig. 15. Surprisingly, Bovy & Tremaine find a steeper force gradient than our standard model, yet derive a smaller dark matter density from it. They underestimate the surface density (cf. Fig. 11), and hence the local dark matter density, because they use the oversimple conversion from K_z to density mentioned above.

Bovy & Rix (2013) used quasi-isothermal DFs to derive the estimates of K_z plotted in Fig. 16 from several populations within the sample of G dwarfs studied by Lee et al. (2011) as part of *SEGUE*. Each 'mono-abundance' population comprises stars that lie in a small bin in the (α/Fe/[Fe/H]) plane and consists of a couple of hundred stars at most. Bovy & Rix (2013) derived an independent gravitational potential and quasi-isothermal DF for each sub-population by requiring that the population's vertical kinematics and spatial distribution are consistent with the observations. They argued that each population constrained K_z at a particular radius, and each point in Fig. 16 shows the constraint provided by one population at the corresponding radius. Since the chemical information we have for our much larger sample of stars is associated with large uncertainties, and we are sceptical that individual mono-abundance populations have quasi-isothermal DFs, we have used a much simpler, metallicity-blind, approach to the data in which it is fundamental that all stars move in the same gravitational potential. None the less, in the region $R > 6.6$ kpc, where the available data are most clearly relevant, the Bovy & Rix points fall nicely within our region of systematic uncertainty, shaded grey in Fig. 16.

Downloaded from https://academic.oup.com/mnras/article-abstract/445/3/3133/1052064
by University of Hull user
on 29 June 2018

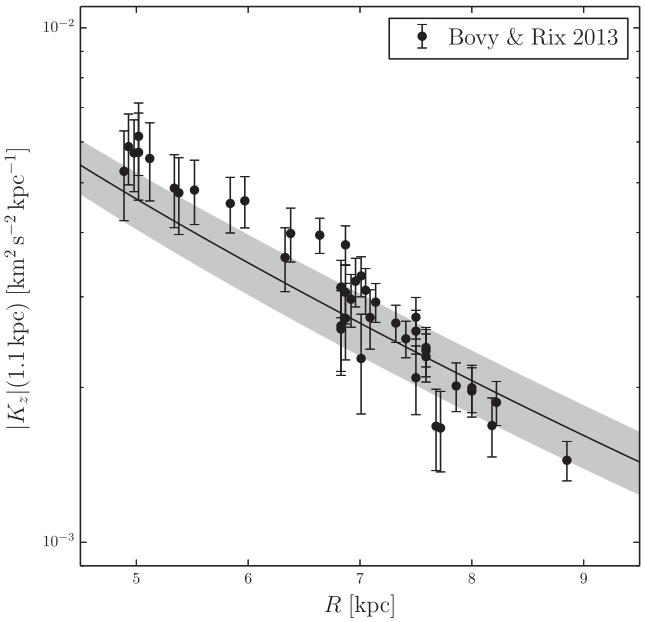

Figure 16. Data points: estimates of $K_z(R, 1.1\,\mathrm{kpc})$ obtained by Bovy & Rix (2013) for mono-abundance populations within the *SEGUE* survey. The black line and the grey-shaded area indicate our best-fitting model and uncertainty.

6.2 Structural parameters of the discs

Our values for the parameters defining the vertical mass profile of the Galactic disc are systematically lower than the canonical values of 300 pc for the thin disc and 900–1400 pc for the thick disc (Gilmore & Reid 1983, J08). One should keep in mind, however, that these values, together with the normalization parameter f_{thk}, are not fully constrained by the data and their uncertainties. It is well known, that extremely similar profiles are produced by parameter values that fall in an extended region of parameter space (e.g. J08).

With our model we do not suffer from this degeneracy in the sense that our values for z_{thn} and z_{thk} are fixed during the alignment of the DF and the mass model, which is done by comparing smooth curves that have no uncertainties. Since we are obtaining good fits to the J08 data (and the Gilmore & Reid 1983 data), there can necessarily be no significance in any difference of the parameters.

6.3 Baryonic mass content

Flynn et al. (2006) find the total luminosity surface density at the Sun in the I band to be $29.5\,\mathrm{L_\odot\ pc^{-2}}$ with an uncertainty of 10 per cent. Combining this with our results we find a total luminosity of the stellar disc of $(3.95 \pm 0.15) \times 10^{10}\,\mathrm{L_\odot}$. With an additional contribution of $10^{10}\,\mathrm{L_\odot}$ from the bulge (Kent, Dame & Fazio 1991; Flynn et al. 2006), we arrive at a total luminosity $L_I \simeq 5 \times 10^{10}\,\mathrm{L_\odot}$ ($M_I \simeq -22.4$) and an I-band mass-to-light ratio of (1.4 ± 0.2). These values are very similar to analogous estimates by Flynn et al. (2006, $M_I \sim -22.3$, $(M/L)_I \sim 1.3$) and Bovy & Rix (2013, $M_I \sim -22.5$, $(M/L)_I \sim 1.3$).

6.4 Consistency with ΛCDM

During our model fitting process, we apply a prior in the concentration parameter c of the dark matter halo that was based on cosmological simulations of structure formation (Section 2.5). There are, however, several other constraints that have to be satisfied and our best-fitting model has a concentration $\ln(c) = 3.0$ that is almost 3σ above the central value of the prior. A similar result was already obtained by McMillan (2011). This illustrates that the additional information from this prior was overruled and, indeed, our results do not change significantly when we use a flat prior instead.

At first glance this seems to point to a mild tension with the predictions from ΛCDM cosmology. One has to keep in mind, however, that the above-mentioned simulations were dark-matter-only runs. The formation of galaxies in the centres of the dark matter haloes will alter their shapes and radial profiles. The classic halo response model of Blumenthal et al. (1986), which assumes an adiabatic contraction of the radial mass profile, is now thought to overpredict the response (e.g. Gnedin et al. 2004, 2010; Abadi et al. 2010). There is also general agreement that there is no universal response that depends only on the final distribution of the baryons, but that the response also depends on the specific accretion history of the Galaxy (Abadi et al. 2010; Gnedin et al. 2010).

Instead of looking at the global shape of the halo, we can compare the predictions of numerical simulations with our robust result on the dark mass contained within the solar radius, $M_{\mathrm{dm}}(r < R_0)$ – a similar approach was taken by Navarro & Steinmetz (2000) and Abadi et al. (2010). We use the mass–concentration relation reported by Macciò, Dutton & van den Bosch (2008),

$$\log c_{200} = 0.917 - 0.104 \log(M_{200}[10^{12} h^{-1}\,\mathrm{M_\odot}]), \qquad (24)$$

with $h = 0.73$, to compute $M_{\mathrm{dm}}(r < R_0)$ as a function of halo mass M_{200} as follows. Given M_{200}, we find c_{200} from equation (24) and compute the mass interior to R_0 in a standard NFW model. For the contracted profiles, we first tabulate the standard NFW mass profile and then contract it according to the prescriptions of Springel & White (1999) (adiabatic) and Abadi et al. (2010) using the baryonic disc and bulge configurations from our best-fitting model. The mass interior to R_0 can then be obtained by interpolation. The cosmic scatter around the relation (24) is well approximated by a lognormal distribution and Macciò et al. (2008) find $\sigma_{\log c} = 0.105$ and hence we obtain a probability distribution for $M_{\mathrm{dm}}(r < R_0)$ for each M_{200}. We can then integrate over a plausible range of Milky Way masses to obtain a probability distribution for $M_{\mathrm{dm}}(r < R_0)$ for our Galaxy. We choose a flat prior between 0.5 and $2 \times 10^{12}\,\mathrm{M_\odot}$ that roughly covers the range of Milky Way masses reported in the literature. Fig. 17 shows the results. If we assume the original NFW profile, we find our model to be a mild outlier as expected from the stronger concentration. Note that in contrast to Abadi et al. (2010) we find that the Milky Way has *more* mass inside R_0 than predicted by cosmology. If we modify the mass profile via adiabatic contraction or the prescription for an intermediate contraction advocated by Abadi et al. (2010), we find much better agreement. The old age of the Galaxy's thin disc implies that our Galaxy has avoided significant mergers for >8 Gyr. Abadi et al. (2010) speculated that in such a case the dark halo would contract more strongly than predicted by their formula. We also note, that Gnedin et al. (2004, 2010) generally predict a contraction that is closer to the adiabatic case than Abadi et al. (2010). Hence, when halo contraction is taken into account we are in excellent agreement with the Milky Way being a typical spiral galaxy in a ΛCDM universe.

7 CONCLUSIONS

We have explored the vertical profile of mass density within ∼1.5 kpc of the Galactic plane by combining the kinematics of ∼200 000 giant stars in the RAVE survey with estimates of the

Downloaded from https://academic.oup.com/mnras/article-abstract/445/3/3133/1052064
by University of Hull user
on 29 June 2018

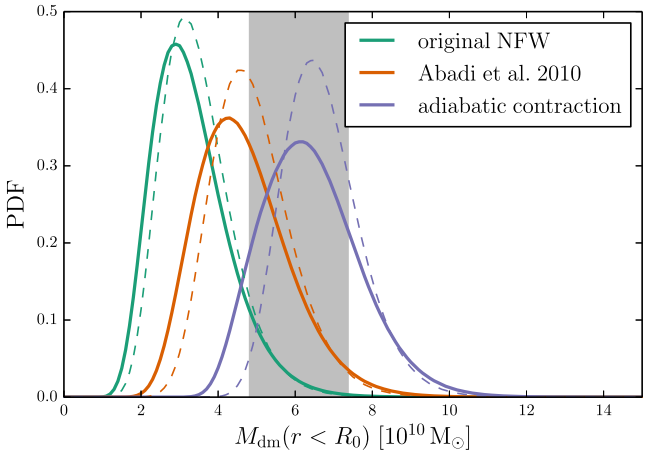

Figure 17. pdfs for $M_{\rm dm}(r < R_0)$ in the ΛCDM cosmology for galaxies with virial masses between 0.5–2 × $10^{12}\,{\rm M}_\odot$. The different lines show the predictions when different degrees of contraction due to the formation of central galaxies in the dark haloes are taken into account. The grey shaded area marks the result of our study. The dashed lines show the predictions for a virial mass equal to our best-fitting value. These are shifted to higher value, because our best-fitting value of 1.3 × $10^{12}\,{\rm M}_\odot$ is slightly on the high side of the above mass range.

variation with z in the number density of disc stars determined by J08 from the SDSS. We have done this using a novel approach to dynamics in which for a given mass model we fit a parametric DF of the form $f(\boldsymbol{J})$ to the kinematics, and then compute the vertical density profile predicted by the chosen DF. This process is repeated using different mass models until the predicted stellar density profile agrees with the observed one.

That we are able to obtain excellent agreement between the predicted and observed stellar profiles is a non-trivial result, and suggests (a) that the parametric form of the DF with which we have chosen to work is capable of approximating the true DF quite accurately, and (b) that our mass models have an appropriate form. The latter comprise double-exponential discs for the ISM, the thin and thick stellar discs plus a NFW dark matter halo and a bulge with spheroidal equidensity surfaces.

While the data we use here constrain tightly the vertical structure of the disc, other data constrain the Galaxy's radial structure better. Consequently, we have determined the radial scalelengths of the density profiles of both the discs and the dark halo from measurements of the proper motion of Sgr A*, terminal velocities of gas inside the Sun, and six-dimensional phase-space coordinates of maser sources. Our models fit these data to well within the errors. The radial scales R_σ on which the velocity-dispersion parameters σ_r of and σ_z of the thin and thick discs decrease with radius have to be extracted from the RAVE data. For the thick disc, the RAVE data yield a reasonable value of R_σ, but they do not yield credible values of R_σ for the thin disc because the survey does not probe the thin disc over a large enough radial range. The low-latitude infrared survey *APOGEE* (Allende Prieto et al. 2008) should resolve this issue, but to date it has not yielded physically plausible results (Bovy et al. 2012b). Consequently, we have simply imposed $R_\sigma = 9\,{\rm kpc}$ to ensure that the thin disc has a roughly radius-independent scaleheight.

The star samples we are using are so large that statistical errors are insignificant, so the uncertainties in our results are entirely systematic. By far the biggest source of uncertainty are the solar distance to the GC and systematic errors in the distances employed in the determination of both the kinematics and the density profile. J08 used a colour–magnitude relation to determine the density of M dwarfs stars. The profile constructed in this way, which is in excellent agreement with the original Gilmore & Reid (1983) profile, is expected to be steeper than the true profile because the observed stars are on average more luminous than they appear to be on account of both Malmquist bias and undiagnosed binarity. We have allowed for these effects by imposing them on our models, using the photometric errors quoted by J08 and a 10 per cent binary fraction. If one uses distances that are 20 per cent too small, one derives a local dark matter density $\rho_{\rm dm,\odot}$ that is ∼8 per cent too low. Similarly, decreasing the assumed value of R_0 from 8.3 to 8 kpc causes $\rho_{\rm dm,\odot}$ to decrease by ∼5 per cent.

What we are really measuring is the vertical profile of gravitating matter, regardless of whether it is baryonic or dark. If we flatten an initially spherical dark halo to axis ratio $q < 1$ while holding constant its mass, the contribution of the halo to the radial force on the Sun rises, as does the halo's contribution to the vertical force that keeps disc stars near the plane. Consequently, to keep our model consistent with the data, the mass of the baryonic disc has to decrease if one decides to use a flattened halo. Hence, flatter haloes require lower mass baryonic discs. In fact, one finds that as the halo is flattened, its mass also has to decrease slightly if the data are to be fitted perfectly, so $\rho_{\rm dm,\odot} \propto q^{-0.89}$ rather than the relation $\rho_{\rm dm,\odot} \propto q^{-1}$ that would apply if the dark-halo mass were independent of q. The surface density within $|z| = 0.9\,{\rm kpc}$ is $69 \pm 15\,{\rm M}_\odot\ {\rm pc}^{-2}$ independent of halo flattening.

With a spherical halo, the total local surface density of the baryonic disc is $37\,{\rm M}_\odot\ {\rm pc}^{-2}$ in excellent agreement with the estimate of Flynn et al. (2006), and the baryons contribute 46 per cent of the radial force on the Sun. The virial mass of the halo is $M_{200} = (1.3 \pm 0.1) \times 10^{12}\,{\rm M}_\odot$ and the mass of the Galaxy's baryons is $(5.6 \pm 1.6) \times 10^{10}\,{\rm M}_\odot$, giving a baryon fraction (stars and cold gas) as small as (4.3 ± 0.6) per cent.

We have used our models to predict the kinematics of hot dwarf stars under the assumption that these stars faithfully sample the contribution to the thin-disc DF from stars with ages <5 Gyr. In the cores of the velocity histograms, the predictions agree well with the RAVE data, but there is a tendency for the wings to be underpredicted by the models, so the division of the overall DF into thin- and thick-disc components may be imperfect, with the young thin disc being slightly colder than it should be. On the other hand, the models predict slightly lower mean-streaming velocities than implied by the data, which is the opposite of what one would expect if the thin disc were too cold. So in subsequent work, it may be necessary to adopt a more complex functional form for the DF.

The fundamental assumption underlying our work is that RAVE stars sample the same population as that probed by J08 and Gilmore & Reid (1983). The worrying aspect of this assumption is that we have used giants from RAVE, whereas J08 and Gilmore & Reid used dwarfs. We do have the reassurance that Binney et al. (2014b) found the kinematics of cool dwarfs and giants to be consistent with one another in RAVE. However, it would be safer to compare the kinematics of the RAVE giants to estimates of the density profile that one derives from them, and we plan to do that soon. In this connection, it will be valuable to derive the density profile from a mixture of the 2MASS and SDSS surveys since SDSS stars are too faint to sample the thin disc well.

In this paper, we have fitted models to the data in phase space rather than the space of the observables (proper motions, parallaxes, magnitudes, etc.). More robust handling of errors is possible if one

Downloaded from https://academic.oup.com/mnras/article-abstract/445/3/3133/1052064
by University of Hull user
on 29 June 2018

fits in the space of observables (McMillan & Binney 2013), and we hope to use the RAVE data in this way soon.

ACKNOWLEDGEMENTS

The research leading to these results has received funding from the European Research Council under the European Union's Seventh Framework Programme (FP7/2007-2013)/ERC grant agreement no. 321067.

Funding for RAVE has been provided by the Australian Astronomical Observatory; the Leibniz-Institut für Astrophysik Potsdam (AIP); the Australian National University; the Australian Research Council; the French National Research Agency; the German Research Foundation (SPP 1177 and SFB 881); the European Research Council (ERC-StG 240271 Galactica); the Istituto Nazionale di Astrofisica at Padova; The Johns Hopkins University; the National Science Foundation of the USA (AST-0908326); the W. M. Keck foundation; the Macquarie University; the Netherlands Research School for Astronomy; the Natural Sciences and Engineering Research Council of Canada; the Slovenian Research Agency; the Swiss National Science Foundation; the Science & Technology Facilities Council of the UK; Opticon; Strasbourg Observatory; and the Universities of Groningen, Heidelberg and Sydney. The RAVE website is at http://www.rave-survey.org.

Figs 11, 10, 15 and 17 were produced using colour schemes from http://www.colorbrewer2.org.

REFERENCES

Abadi M. G., Navarro J. F., Fardal M., Babul A., Steinmetz M., 2010, MNRAS, 407, 435
Allende Prieto C. et al., 2008, Astron. Nachr., 329, 1018
Antoja T. et al., 2012, MNRAS, 426, L1
Aumer M., Binney J. J., 2009, MNRAS, 397, 1286
Bershady M. A., Martinsson T. P. K., Verheijen M. A. W., Westfall K. B., Andersen D. R., Swaters R. A., 2011, ApJ, 739, L47
Bienaymé O., Soubiran C., Mishenina T. V., Kovtyukh V. V., Siebert A., 2006, A&A, 446, 933
Bienaymé O. et al., 2014, preprint (arXiv:1406.6896)
Binney J., 2010a, MNRAS, 401, 2318
Binney J. J., 2010b, in Falcón-Barroso J., Knapen J. H., eds, Secular Evolution of Galaxies. Cambridge Univ. Press, Cambridge, p. 141
Binney J., 2012a, MNRAS, 426, 1324
Binney J., 2012b, MNRAS, 426, 1328 (B12b)
Binney J., 2014, MNRAS, 440, 787
Binney J., Merrifield M., 1998, Galactic Astronomy. Princeton Univ. Press, Princeton, NJ
Binney J., Gerhard O., Spergel D., 1997, MNRAS, 288, 365
Binney J. et al., 2014a, MNRAS, 437, 351
Binney J. et al., 2014b, MNRAS, 439, 1231
Bissantz N., Gerhard O., 2002, MNRAS, 330, 591
Blumenthal G. R., Faber S. M., Flores R., Primack J. R., 1986, ApJ, 301, 27
Bond N. A. et al., 2010, ApJ, 716, 1
Bovy J., Rix H. W., 2013, ApJ, 779, 115
Bovy J., Tremaine S., 2012, ApJ, 756, 89
Bovy J., Rix H. W., Liu C., Hogg D. W., Beers T. C., Lee Y. S., 2012a, ApJ, 753, 148
Bovy J. et al., 2012b, ApJ, 759, 131
Bower R. G., Vernon I., Goldstein M., Benson A. J., Lacey C. G., Baugh C. M., Cole S., Frenk C. S., 2010, MNRAS, 407, 2017
Boylan-Kolchin M., Springel V., White S. D. M., Jenkins A., 2010, MNRAS, 406, 896
Caldwell J. A. R., Ostriker J. P., 1981, ApJ, 251, 61
Das P., Gerhard O., Mendez R. H., Teodorescu A. M., de Lorenzi F., 2011, MNRAS, 415, 1244
Debattista V. P., 2014, MNRAS, 443, L1
Dehnen W., 1998, AJ, 115, 2384
Dehnen W., Binney J., 1998, MNRAS, 294, 429
Delfosse X. et al., 2004, in Hilditch R. W., Hensberge H., Pavlovski K., eds, ASP Conf. Ser. Vol. 318, Spectroscopically and Spatially Resolving the Components of the Close Binary Stars. Astron. Soc. Pac., San Francisco, p. 166
Dieterich S. B., Henry T. J., Golimowski D. A., Krist J. E., Tanner A. M., 2012, AJ, 144, 64
Faure C., Siebert A., Famaey B., 2014, MNRAS, 440, 2564
Flynn C., Holmberg J., Portinari L., Fuchs B., Jahreiß H., 2006, MNRAS, 372, 1149
Garbari S., Liu C., Read J. I., Lake G., 2012, MNRAS, 425, 1445
Gillessen S., Eisenhauer F., Fritz T. K., Bartko H., Dodds-Eden K., Pfuhl O., Ott T., Genzel R., 2009, ApJ, 707, L114
Gilmore G., Reid N., 1983, MNRAS, 202, 1025
Gnedin O. Y., Kravtsov A. V., Klypin A. A., Nagai D., 2004, ApJ, 616, 16
Gnedin O. Y., Brown W. R., Geller M. J., Kenyon S. J., 2010, ApJ, 720, L108
Guo Q., White S., Li C., Boylan-Kolchin M., 2010, MNRAS, 404, 1111
Hinshaw G. et al., 2013, ApJS, 208, 19
Holmberg J., Flynn C., 2004, MNRAS, 352, 440
Holmberg J., Nordström B., Andersen J., 2007, A&A, 475, 519
Iocco F., Pato M., Bertone G., Jetzer P., 2011, J. Cosmol. Astropart. Phys., 11, 029
Jurić M. et al., 2008, ApJ, 673, 864 (J08)
Kahn F. D., Woltjer L., 1959, ApJ, 130, 705
Kent S. M., Dame T. M., Fazio G., 1991, ApJ, 378, 131
Klypin A., Kravtsov A. V., Valenzuela O., Prada F., 1999, ApJ, 522, 82
Kneib J. P., Natarajan P., 2011, A&AR, 19, 47
Korchagin V. I., Girard T. M., Borkova T. V., Dinescu D. I., van Altena W. F., 2003, AJ, 126, 2896
Kordopatis G. et al., 2013, AJ, 146, 134
Kuijken K., Gilmore G., 1991, ApJ, 367, L9
Lee Y. S. et al., 2011, ApJ, 738, 187
Li Y. S., White S. D. M., 2008, MNRAS, 384, 1459
Macciò A. V., Dutton A. A., van den Bosch F. C., 2008, MNRAS, 391, 1940
McMillan P. J., 2011, MNRAS, 414, 2446
McMillan P. J., Binney J. J., 2010, MNRAS, 402, 934
McMillan P. J., Binney J. J., 2013, MNRAS, 433, 1411
Malhotra S., 1995, ApJ, 448, 138
Marinacci F., Binney J., Fraternali F., Nipoti C., Ciotti L., Londrillo P., 2010, MNRAS, 404, 1464
Martinsson T. P. K., Verheijen M. A. W., Westfall K. B., Bershady M. A., Andersen D. R., Swaters R. A., 2013, A&A, 557, A131
Mirabolfathi N., 2013, preprint (arXiv:1308.0044)
Moni Bidin C., Carraro G., Méndez R. A., 2012a, ApJ, 747, 101
Moni Bidin C., Carraro G., Méndez R. A., Smith R., 2012b, ApJ, 751, 30
Navarro J. F., Steinmetz M., 2000, ApJ, 528, 607
Navarro J. F., Frenk C. S., White S. D. M., 1996, ApJ, 462, 563
Nesti F., Salucci P., 2013, J. Cosmol. Astropart. Phys., 7, 016
Nordström B. et al., 2004, A&A, 418, 989
Piffl T. et al., 2014, A&A, 562, A91
Planck Collaboration XVI, 2013, preprint (arXiv:1303.5076)
Press W. H., Teukolsky S. A., Vetterling W. T., Flannery B. P., 2007, Numerical Recipes 3rd edn: The Art of Scientific Computing. Cambridge Univ. Press, New York, NY
Read J. I., 2014, J. Phys. G Nucl. Phys., 41, 063101
Reid M. J., Brunthaler A., 2004, ApJ, 616, 872
Reid M. J. et al., 2014, ApJ, 783, 130
Sackett P. D., 1997, ApJ, 483, 103
Salucci P., Nesti F., Gentile G., Frigerio Martins C., 2010, A&A, 523, A83
Sanders J. L., 2012, MNRAS, 425, 2228
Schönrich R., 2012, MNRAS, 427, 274
Schönrich R., Bergemann M., 2014, MNRAS, 443, 698
Schönrich R., Binney J., Dehnen W., 2010, MNRAS, 403, 1829
Siebert A. et al., 2012, MNRAS, 425, 2335
Springel V., White S. D. M., 1999, MNRAS, 307, 162

Downloaded from https://academic.oup.com/mnras/article-abstract/445/3/3133/1052064
by University of Hull user
on 29 June 2018

Steinmetz M. et al., 2006, AJ, 132, 1645
van Albada T. S., Bahcall J. N., Begeman K., Sancisi R., 1985, ApJ, 295, 305
van der Kruit P. C., Searle L., 1981, A&A, 95, 105
Velander M. et al., 2014, MNRAS, 437, 2111
Wilkinson M. I., Evans N. W., 1999, MNRAS, 310, 645
Williams M. E. K. et al., 2013, MNRAS, 436, 101
Yanny B. et al., 2009, AJ, 137, 4377
York D. G. et al., 2000, AJ, 120, 1579
Zacharias N., Finch C. T., Girard T. M., Henden A., Bartlett J. L., Monet D. G., Zacharias M. I., 2013, AJ, 145, 44
Zhang L., Rix H. W., van de Ven G., Bovy J., Liu C., Zhao G., 2013, ApJ, 772, 108

This paper has been typeset from a TEX/LATEX file prepared by the author.

Downloaded from https://academic.oup.com/mnras/article-abstract/445/3/3133/1052064
by University of Hull user
on 29 June 2018